공학박사 학위논문

Reconstruction and Projection of Sea Levels Around the Korean Peninsula Using Cyclo-Stationary Empirical Orthogonal Function

CSEOF 를 이용한 한반도 주변 해역의

해수면 복원 및 전망

2017 년 2 월

서울대학교 대학원

건설환경공학부

천세현

Reconstruction and Projection of Sea Levels Around the Korean Peninsula Using Cyclo-Stationary Empirical Orthogonal Function

CSEOF 를 이용한 한반도 주변 해역의 해수면 복원 및 전망

지도교수 서 경 덕

이 논문을 공학박사 학위논문으로 제출함

2016 년 10 월

서울대학교 대학원

건설환경공학부

천 세 현

천세현의 박사 학위논문을 인준함

2016 년 12 월

위 원 장 서 일 원 (인)

부위원장 서 경 덕 (인)

위 원 김 영 오 (인)

위 원 안 경 모 (인)

위 원 Benjamin Hamlington (인)

Abstract

Reconstruction and Projection of Sea Levels Around the Korean Peninsula Using Cyclo-Stationary Empirical Orthogonal Function

Se-Hyeon Cheon
Department of Civil and Environmental Engineering
The Graduate School
Seoul National University

Since the operating of satellite altimeter, the understanding of the sea level has been increased dramatically. However, the history of the satellite altimeter dates back to the 1990s; it is relatively short compared with the history of tide gauge (TG) observation. Many studies have been conducted to extend the spatial resolution of the satellite data into the time before satellite measurements by using both satellite data and TG data simultaneously. However, most of the reconstructions of sea level were conducted on a global scale, which brought on reducing accuracy at some local areas, where the signal is relatively weaker than other regions and the number of TG is not enough to represent the area. The sea level around the Korean Peninsula is also relatively low signal zone, and the number of TG is few before 1960. Therefore, in this study, new methods are proposed to reconstruct the past sea level and project the future sea level around the Korean Peninsula. Using CSEOF's (Cyclo-Stationary Empirical Orthogonal Function) loading vectors

(LV) of satellite data as basis functions of the reconstruction, the principal component time series (PCT) of LV is extended over 1900-2014. The PCTs of sea surface temperature data and altimeter data are used as independent variables and depending variables for regression analysis, respectively. The regression analysis considering time lags is conducted to find the lags and regression coefficients. Using the regression results, the PCTs of satellite data were extended into the past. In this study, we conducted 13 reconstructions; and COBESST2 data of the North-west Pacific Ocean showed the best agreement with TG observations. Although the TG data was not used in the reconstruction process, the reconstructed results showed better agreement with the TG observation than a previous study that used the TG data. The projection of sea level around the Korean Peninsula was conducted as well corresponding to greenhouse gas emission scenarios. The basic concept of the projection was similar to the reconstruction in using the LVs of satellite altimeter data as the basis function, but the projection employed the simulated SST data of HadGEM2-ES to extend the PCTs of the basis functions. The projection was conducted for four RCP scenarios (RCP 2.6, 4.5, 6.0 and 8.5) over 2006-2100. The results in reconstruction and projection were given as both mean and standard deviation for each month and each grid point through Monte Carlo simulations.

Keywords: Sea Level Rise, Satellite Altimetry, SST, Sea Level Reconstruction, Sea Level Projection, CSEOF, Korean Peninsula

Student Number: 2012-30250

Contents

List of Tables

List of Figures

Chapter 1 Introduction

Even though there is some disagreement as to its cause, sea level rise is occurring. Many low-lying areas have been affected by changes in sea level. As a result, coastal communities across the globe have been trying to make proper mitigation and adaptation plans. Therefore it is crucial to understand the sea level change and predict how it will change in the future.

Before starting satellite altimeter era, a scientist had to rely on the tide gauge (after this TG) data. The TG data have been providing the records of local sea level variations, covering a time period of nearly two hundred years. Using TG data, scientists can study past sea level changes at specific locations across the globe. However, TGs do not provide good global coverage with a necessary a bias towards coastal sites and the Northern Hemisphere, and relatively few TGs located near the poles.

Satellite altimeters have been collecting data since 1992. The satellite altimetry data have global coverage of sea level but a relatively short observation period compared to TG observations, which is a severe handicap to analyzing long-term changes in sea level. This is particularly true given the presence of sea level variability with decadal timescales.

Using reduced-space optimal interpolation that combines TGs and satellite altimeter data, the scientists can overcome the detriments of each observation data type. The altimeter data is decomposed into empirically independent basis functions of spatial variability, which are then fit to the TG data set back through time. Through this process a sea level data set is created

that has a spatially high resolution and temporally longer period. In the first reconstructions, Church and White (2006) used empirical orthogonal functions (after this EOF) , but in recent years cyclo-stationary empirical orthogonal function (hereafter CSEOF) have been implemented as the basis of the reconstruction (e.g. Hamlington et al., 2011). The original Church and White (2006) was on a global scale and has been widely used by the scientific community.

However, using this and other global reconstructions around the Korean Peninsula (hereafter KP) have some problems. First, the global scale reconstructions used a limited number of basis functions to prevent interpolation from over-fitting and creating spurious sea level fluctuations. There is a difference between the major modes for global scale and the major modes for local scale; e.g. there is high possibility that the globally selected basis functions, which represent 90 % of the total variance in the global level, will not represent 90 % of the total variance in local scale (see Figure 1.1 and Figure 1.2). Second, the temporal coverage of the TG data around the KP started around 1930 when less than 10 TGs were available; it is too little to secure accuracy on these local scales.

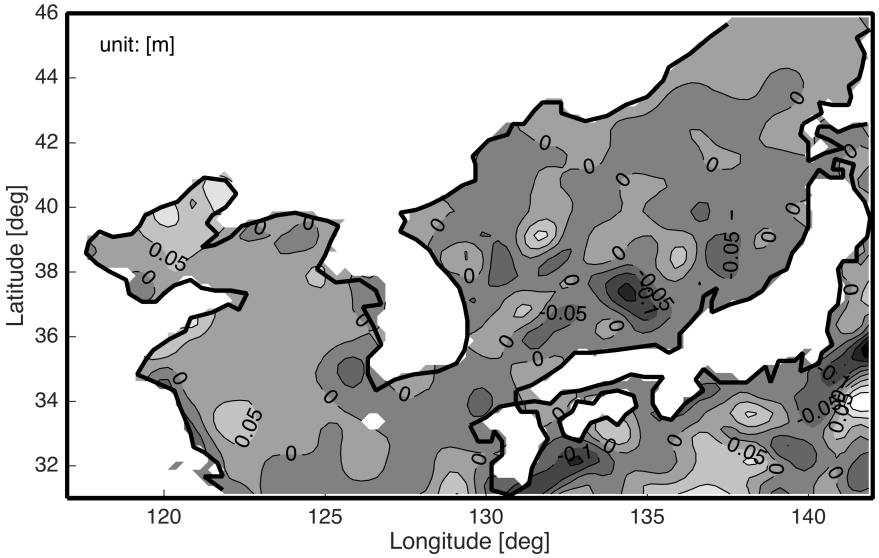

Figure 1.1 Sea level anomaly combining 90% of CSEOF modes of global domain (Jun. 1993)

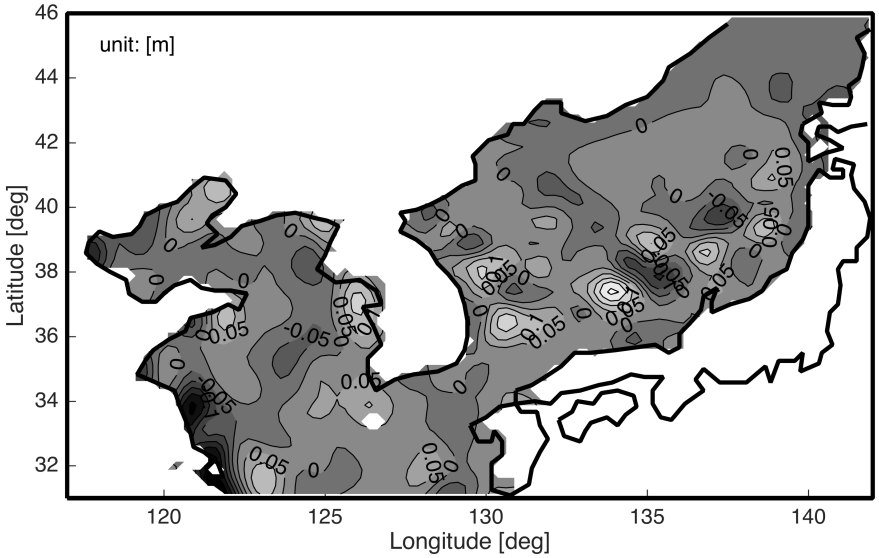

Figure 1.2. Sea level anomaly combining 90% of CSEOF modes of local domain (Jun. 1993)

A projection of the future sea level is positively necessary to properly plan and develop coastal mitigation and adaptation strategies. But the physical explanations for the sea level changes are not advanced enough to make such prediction. The AOGCMs (Atmosphere-Ocean General Circulation Models) of CMIP5 considered only thermal expansion and used a semi-empirical method to separately estimate the surface mass balance; even if we let the model weakness alone, it is likely that the model-based projection of future sea level has large uncertainty, particularly on regional and local scales. For this reason, researchers have primarily been conducting projection studies on a global scale to reduce the inherent uncertainty. On these scales, much of the regional variability in the ocean cancels out or at least has a significantly reduced impact. Unfortunately, the global scale projections are not representative of future local sea level at most locations around the world. It is the local projections that are important for planning and engineering purposes, not the global ones. There are a few studies for regional future sea level projections, but, to date, a study has not been completed for the KP. Therefore, it is necessary to conduct a projection preserving the distinct feature around the KP.

The primary purpose of this study is creating a reconstruction and projection of local sea level anomaly (after this SLA) around the Korean Peninsula. Modified reconstruction and projection schemes are necessary to achieve this goal.

Considering the problems of previous studies and purpose of this study, the research questions of this research is given as follows:

1. What are the characteristics of sea level anomaly around the Korean Peninsula?

2. How can we reconstruct a sea level anomaly when we have very few historical measurements?

3. What is the sea level anomaly around the Korean Peninsula over 1900-2014?

4. How can we project the future sea level anomaly keeping the local characteristics around the Korean Peninsula?

5. What is the sea level anomaly around the Korean Peninsula over 2006-2100?

In chapter 2, we summarize the previous studies that are related to SLA reconstruction and projection. In chapter 3, the data that were used in this study are introduced. The detailed method for current reconstruction and projection is in chapter 4. Next, we show the reconstruction and projection results and their verifications. In chapter 6, we discuss the results and method. Finally, in chapter 7, the summaries and suggestions for future research are written.

Chapter 2 Literature Review

2.1 Sea Level Reconstruction

2.1.1 Introduction

Before starting the detailed discussion on the research completed, a review of past SLA reconstruction efforts is provided here. Altimetry data has very short time coverage (on the order of two decades), and the TG data has poor and biased spatial distribution. Using both satellite altimeter data and historical TG data, researchers have reconstructed past SLA, on both global and local scales. There are several different approaches for the reconstruction and subsequent projection of future sea level. In this chapter, we summarize these methods to provide a better understanding of this research.

2.2.2 Reconstruction from optimal interpolation

To overcome the obvious shortcoming of each data set (TG and satellite altimeter), many researchers have attempted to combine both data sets using a variety of different approaches. One of the popular methods has been an optimal interpolation.

Chambers et al. (2002) attempted to reconstruct SLA combining TG data and satellite altimeter data. In their research, they studied low-frequency variability in global mean sea level (hereafter GMSL) from 1950 to 2000. They interpolated sparse TG data into a global gridded SLA pattern applying EOFs (Empirical Orthogonal Functions) of SLA using TOPEX/Poseidon satellite altimeter to capture the interannual-scale signals, e.g., El Nino-

Southern Oscillation (hereafter ENSO) and the Pacific Decadal Oscillation (from now on PDO). The reconstruction has 2-4 mm RMS accuracy for a 1-year running mean smoothing and about 1mm for a 5-year running mean smoothing. Reconstructed GMSL shows a rising trend throughout the 1990s.

Based on the previous studies (Chambers et al., 2002; Kaplan et al., 1998; Kaplan et al., 2000), (Church et al., 2004) provided a reconstruction from 1950 to 2001 using EOFs of SLA data measured from satellite altimeter and reduced space optimal interpolation scheme. This research was subsequently updated to increase temporal coverage from 1870 to the present (Church and White, 2006, 2011) and the reconstructions have been made available to the public. The GMSL rose about 210 mm from 1880 to 2009, and the linear trend over 1900-2009 is 1.7 ± 0.2 mm per year. The resulting SLA is one of the most comprehensive and widely cited reconstructions (Hamlington et al., 2012a).

Hamlington et al. (2011) applied cyclo-stationary empirical orthogonal functions as basis functions for the reconstruction of SLA instead of EOFs. This approach provides an advantage for describing local variations such as ENSO and PDO. After that, Hamlington et al. (2012a) proposed an improving scheme of their reconstruction using sea surface temperature (hereafter SST).

Given the limited TG data in the past, reconstructions of sea level relying only on TGs are poor, particularly before 1950. Leveraging other ocean observations (e.g. SST) to reconstruct sea level leads to an improved sea level reconstruction further into the past.

2.2.3 Reconstruction using numerical model

Bergé-Nguyen et al. (2008) reconstructed SLA over 1950 to 2003 using TG data and EOFs of different spatial data. The sources follow: (1) thermosteric sea level grids over 1955-2003, (2) sea level grids from T/P satellite altimetry over 1993-2003, and (3) dynamic height grids from the SODA (Simple Ocean Data Assimilation) reanalysis over 1958-2001 (Carton et al., 2005). Among the three reconstructions, the second case showed the most similar results to the observed SLA.

Llovel et al. (2009) proposed a two-dimensional reconstruction of past sea level over 1950-2003 using TG data and 2-degree sea level grids data from the OPA/NEMO (Océan PArallélisé, Nucleus for European Modelling of the Ocean) OGCM (ocean general circulation model). An EOF decomposition of the model data had two main modes: (1) a multi-decadal signal and (2) a local interannual signal such as ENSO and PDO. The model matched well for the second case, but the simulated multi-decadal signal showed very sensitive behavior to the simulation time span.

Meyssignac et al. (2012) compared different past sea level reconstructions to investigate the influence of the chosen spatial modes used to constrain the reconstruction and the period covered by the corresponding gridded sea level time series over 1950-2009. They used both a pure physical ocean circulation model (DRAKKAR/NEMO; Barnier et al. (2007)) without data assimilation and an ocean reanalysis model (SODA; Carton and Giese (2008)) over 1958-2007. They found that the reconstructed GMSL did not depend on the input spatial grids much but depend on TG data. EOFs of each gridded data showed very sensitive behavior to gridded input data.

And to conclude, a review of previous studies reveals that the current numerical skills do not simulate past sea level changes well.

2.2.4 Probabilistic reconstruction

Choblet et al. (2014) presented a new reconstruction method, which applied a Bayesian inference method. They did not focus on climate-related variations but concentrated on rates of change of SLA.

Hay et al. (2015) focused on disagreements between GMSL and the change of individual contributors such as glacier and ice-sheet mass loss, thermal expansion of sea water, and changes in land water storage over 1900-1990. To explain the difference, Hay et al. (2015) revisited the GMSL rise over twentieth-century using probabilistic method (Hay et al., 2013; Kopp, 2013) they found the GMSL rising ratio as 1.2 ± 0.2 mm per year with 90% confidence interval over 1901-1990.

The probabilistic reconstruction scheme is still in the developing stages, but so far their results are different from other reconstructions; this means that more research is necessary to determine which approach is the best and results in the most accurate reconstruction.

2.2.5 Regional sea level reconstruction

While most of the research has been conducted based on global reconstructions, several studies have instead focused on regional reconstructions of sea level. Using an optimal interpolation method, Calafat and Gomis (2009) reconstructed the distribution of SLA in the Mediterranean

Sea over 1945-2000. They used EOFs of satellite altimeter data spanning 1993-2005 as basis functions and interpolated these basis functions into TG data. A spatial distribution of sea level rise trends for the period of 1945-2000 indicated a positive trend in most areas. A strong positive trend showed up in the Ionian Sea (up to 1.5 mm per year), and a negative peak appeared in the southeast of Crete (up to -0.5 mm per year). The reconstructions in an open-sea region with little correlation between TG and satellite altimeter data were poor.

Calafat et al. (2009) compared their reconstruction to reanalysis results from OPA (Ocean PArallelise) model (Delecluse et al., 1998) that is 3D (baroclinic) regional circulation model over 1961-2000. They found the numerical simulations could not simulate well the interannual sea level changes such as the Eastern Mediterranean Transient. Calafat and Jordà (2011) extended the reconstruction period up to 2008; from their error budget estimating, they concluded that the baseline error that was due to the truncation of the EOFs was the dominant error in their reconstruction.

Hamlington et al. (2012b) performed a regional sea level reconstruction based on the scheme applying CSEOFs (Hamlington et al., 2011); and their local domain was the Pacific Ocean. They found that a choice of basis functions had a significant effect on the spatial pattern of the sea level rising trend.

2.2.6 Conclusion

Many researching groups proposed sea level reconstructions using different schemes: optimal interpolation, numerical simulation, probabilistic method.

Each study showed good agreement for satellite altimeter era (1993-current), but not for the earlier period over 1900-1993; the trends of GMSLs of the reconstructions results were similar, but the spatial patterns of the reconstructions were not.

Most of the research focused on a global scale reconstruction, and the local reconstruction applied the same method as the global reconstruction. However, the regional sea level changes are different from the changes in GMSL. Hence, more studies of regional-based reconstruction and schemes are necessary.

2.2 Future sea level projection

Studies relating to the future sea level projection dated back to the 1980s (Hoffman, 1984; Hoffman et al., 1983; Oerlemans, 1989; Patwardhan and Small, 1992; Van der Veen, 1988). Following this initial research, researchers have conducted lots of studies with the various viewpoints. Among the studies, the sea-level rise chapter (Church et al., 2013) of the Intergovernmental Panel on Climate Change (IPCC) Fifth Assessment Report (AR5) introduced and assessed various projection results. In this section, the recent researches about projecting future sea level are summarized.

Most of the studies relating to the future sea level projection were conducted on a global scale because an Earth climate system can be considered as a closed system in the view of a water mass. Therefore researchers can focus on the change of land ice mass and the thermal expansion of the ocean because the most of the net energy increase in the Earth's climate system is stored in the ocean in the form of heat (Slangen et al., 2016).

IPCC AR5 (Stocker et al., 2013) suggested the future sea level scenarios for each RCP (Representative Concentration Pathways) scenario, based on the process-based projections resulting from 21 CMIP5 Atmosphere-Ocean General Circulation Models (AOGCMs). To project future sea level, they combined various sea level changes caused by each source such as GMSL from thermal expansion and GMSL from the surface mass balance change. The project GMSL were as follows: 44 ± 17 cm (RCP2.6), 53 ± 18 cm (RCP4.5), 55 ± 18 cm (RCP6.0), and 74 ± 23 cm (RCP8.5).

After IPCC AR5 was published lots of research adopted CMIP5 climate models to conduct regional sea level projection (Bilbao et al., 2015; Bouttes and Gregory, 2014; Kopp et al., 2014; Little et al., 2015; Slangen et al., 2014). Using the CMIP5 climate models results, the studies are separated into two branches. First group combined the CMIP5 results with the offline models to compute local sea level change (de Vries et al., 2014; Han et al., 2014; Han et al., 2015; Simpson et al., 2014; Slangen et al., 2014; Slangen et al., 2012). The others tried to provide complete probability distributions of local sea level.

Chapter 3 Data

A sea level anomaly around the Korean Peninsula (hereafter SLA-KP), SST, and the wind on the North-West Pacific (hereafter NWP) data are needed to perform the current regional reconstruction. Every data set is gridded to conduct CSEOF decomposition. The CSEOFs of SLA-KP are to be basis functions for the SLA-KP reconstruction. The CSEOFs of SST and wind data play a role as independent variables to extend principle component time-series (hereafter PCT) of SLA's CSEOFs into the past. The TG data is not necessary for the reconstruction process. However, it is in use to verify the result.

3.1 Tide gauge data

Monthly mean sea level records of 47 TGs obtained from the Permanent Service for Mean Sea Level (hereafter PSMSL). The Revised Local Reference (RLR) data are selected; the RLR data are measured sea levels at each site about a constant local datum over the complete record. Hereafter, TG data sets around the Korean Peninsula are named as TGs_KP.

A temporal coverage for this study is from 1900 to 2014. However, the earliest data of TGs_KP is traced back to 1930 at Wajima Station (see Figure 3.1 and Table 1), and the latest data is up to 2013. The forty-seven TGs_KP downloaded from PSMSL over 1930-2013 (see Table 1).

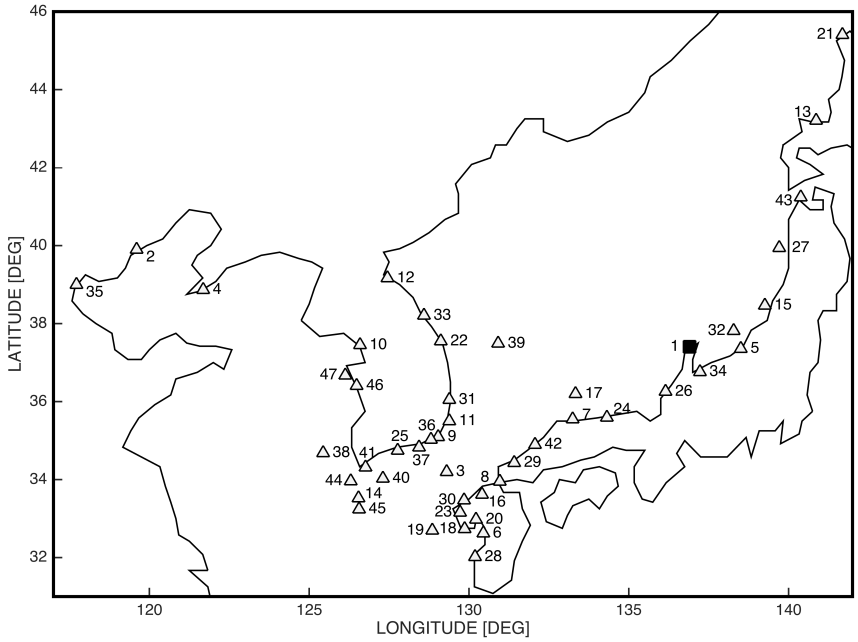

Figure 3.1 TG locations around the Korean Peninsula. The black square is Wajima TG station which has the longest record length (1930-present)

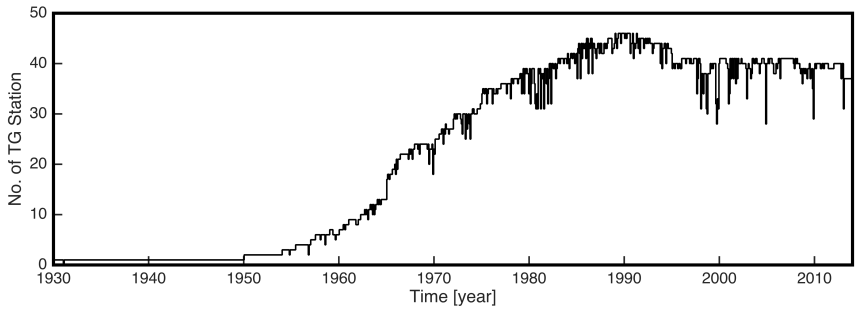

Figure 3.2 Time series of available TG data around the KP

Before 1965, the number of available TGs_KP is less than 10, and there is only one TG data set exist earlier than 1950. Most of TGs_KP are available from 1970 (Figure 3.2).

An ongoing GIA (glacial isostatic adjustment) effect was removed from TG data using ICE-5G VM2 model (Peltier, 2004); see Figure **3**.**3**. Because an IB (Inverted Barometer) correction was applied to the satellite altimetry data, the TG data are modified by IB correction based on the pressure fields from 20th Century Reanalysis V2c data (Compo et al., 2006; Compo et al., 2011; Hirahara et al., 2014; Whitaker et al., 2004), which is provided by the NOAA/OAR/ESRL PSD, Boulder, Colorado, USA, from their Web site at http://www.esrl.noaa.gov/psd/.

The TGs used in this study are selected with a particular editing criteria. The technique for editing the TGs are obtained by the following procedures, similar to those of (Hamlington et al., 2011). In summary, TGs, which had short record length and unphysical variations such as uncorrectable vertical land motion, are removed. After calculating a month-to-month change, records which are greater than 250 mm are removed.

Table 1. Information of TG Stations

ID	Lon.	Lat.	Name	ID	Lon.	Lat.	Name
1	136.9	37.406	WAJIMA	25	127.766	34.747	YEOSU
2	119.6	39.9	QINHUANGDAO	26	136.149	36.255	MIKUNI
3	129.3	34.2	IZUHARA	27	139.706	39.942	OGA
4	121.683	38.867	DALIAN	28	130.191	32.018	AKUNE
5	138.508	37.357	KASHIWAZAKI	29	131.417	34.433	HAGI
6	130.451	32.623	MISUMI	30	129.849	33.473	KARIYA
7	133.243	35.548	SAKAI	31	129.384	36.047	POHANG
8	130.967	33.95	MOZI	32	138.281	37.815	OGI
9	129.036	35.096	BUSAN	33	128.594	38.207	SOKCHO
10	126.592	37.452	INCHEON	34	137.225	36.762	TOYAMA
11	129.387	35.502	ULSAN	35	117.717	39	TANGGU
12	127.45	39.167	WONSAN	36	128.811	35.025	GADEOKDO
13	140.858	43.209	OSHIRO II	37	128.435	34.828	TONGYEONG
14	126.543	33.528	JEJU	38	125.436	34.684	DAEHEUKSANDO
15	139.255	38.468	AWA SIMA	39	130.914	37.491	ULLEUNG
16	130.408	33.619	HAKATA	40	127.309	34.028	GEOMUNDO
17	133.331	36.201	SAIGO	41	126.76	34.315	WANDO
18	129.866	32.735	NAGASAKI	42	132.066	34.897	HAMADA II
19	128.849	32.696	FUKUE	43	140.381	41.243	TAPPI
20	130.221	32.977	OURA	44	126.3	33.962	CHUJADO
21	141.685	45.408	WAKKANAI	45	126.562	33.24	SEOGWIPO
22	129.116	37.55	MUKHO	46	126.486	36.406	BORYEONG
23	129.724	33.158	SASEBO II	47	126.132	36.674	ANHEUNG
24	134.316	35.594	TAJIRI				

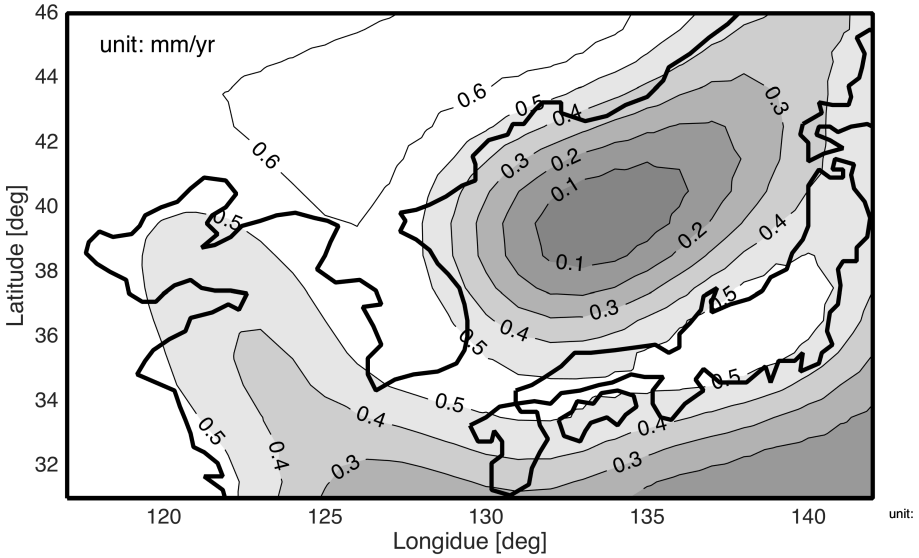

Figure 3.3. Glacial Isostatic Adjustment values around the Korean Peninsula from ICE-5G(VM2).

3.2 Sea Level Anomaly

Basis functions for this reconstruction are the CSEOFs based on a monthly mean gridded SLA. The satellite has measured SLA since 1992. The gridded SLA data sets are available via the AVISO (the Archiving, Validation, and Interpretation of Satellite Oceanographic); this data opens in public (ftp://ftp.aviso.altimetry.fr/global/delayed-time/grids/climatology/monthly_mean/), and hereafter this data set is written as AVISO-SLA. The data is made based on satellite altimeter measurements over 1993-2014; Topex/Poseidon, ERS-1&2, Geosat Follow-On, Envisat, Jason-1&2, and OSTM satellites collected the SLA. The delayed time Ssalto/DUACS multi-mission altimeter data processing system has created this product. Before conducting the CSEOF decomposition, mean values for each grid point were removed to prevent those values to have much influence on CSEOFs. Unlike TG data set, the SLA data don't need to remove the annual signal since CSEOF decomposition separates the yearly sign. The data was trimmed to containing the ocean around the KP only (N31°-46° and E117°-142°; hereafter AVISO-KP) and it was multiplied by the square root of the cosine of latitude to consider the actual area of each grid. All grid points that were not continuous in the temporal level were removed.

3.3 GRACE

The GRACE (GRAVITY RECOVERY & CLIMATE EXPERIMENT) twin satellites are a collaboration of the two space agencies, NASA (US) and DLR (German). Launched 17 March 2002, the GRACE satellites have been measuring Earth's gravity field changes. By analyzing the measured data, many researching groups can estimate not only the changes of water mass over land, ice, and oceans but also earth surface deformations.

The GRACE Ground System consist of three institutes: CSR, GFZ, and JPL; these represent Center for Space Research of the University of Texas, GeoForschungsZentrum Potsdam, and Jet Propulsion Laboratory respectively. They have been producing level-2 data (spherical harmonic fields) and spherical harmonic coefficients of the gravity field. Based on these outputs, level-3 spherical harmonic data versions have been provided by GRACE Tellus program.

In this research, a recent version of monthly averaged GRACE Mascon data (hereafter GRACE-Mascon), released on June 1, 2016, is applied. Applying the mascon (mass concentration) is an alternative approach for gravity changes regarding spherical harmonics. Considering the mascon of each specific area (hereafter Mascon), one can specify that the gravity change of each Mascon, because each Macon has a particular geophysical location. This advantage allows a better separation of land and ocean. This data applied a GIA (glacial isostatic adjustment) correction based on the model (Geruo et al., 2013; Wahr et al., 1998) and an IB correction based on ECMWF (European Centre for Medium-Range Weather Forecasts) atmospheric pressure fields.

3.4 Sea Surface Temperature

PCTs of CSEOFs based on SST data play a role as a predictor (or independent) variable in multiple regression. Instead of directly using of observation data, reanalyzed SST applied to this research because the observation data is sparse in space and discontinuous in time. In this study, four kinds of SST reconstruction data sets were used: ERSST (Extended Reconstructed Sea Surface Temperature) (Huang et al., 2015a; Huang et al., 2015b; Liu et al., 2015), COBESST (Centennial in situ Observation-Based Estimates; Ishii et al. (2005)), COBESST2 Ishii et al. (2005), HadiSST (Hadley Centre Global Sea Ice and Sea Surface Temperature; Rayner et al. (2003)).

The ERSST dataset is a global monthly SST dataset based on the observation of ICOADS (International Comprehensive Ocean–Atmosphere Dataset). This monthly analysis has a 2° × 2° grid resolution and its time coverage is from 1854 to recent time including anomalies computed on a 1971–2000 monthly climatology. The data provided by the NOAA/OAR/ESRL PSD, Boulder, Colorado, USA, from their Web site at http://www.esrl.noaa.gov/psd/.

The COBESST dataset is a monthly interpolated 1°x1° SST product over 1891-present. It integrates several SST observations: ICOADS 2.0, the Japanese Kobe collection, and reports from ships and buoys. The bucket correction process was applied to the data up to 1941 same as HadiSST dataset (Folland and Parker, 1995). The data provided by the NOAA/OAR/ESRL PSD, Boulder, Colorado, USA, from their Web site at http://www.esrl.noaa.gov/psd/.

The COBESST2 dataset is a monthly interpolated 1°x1° SST product over 1850-present. It integrates several SST observations: ICOADS 2.5, satellite SST, and satellite sea ice. The bucket correction process was applied to the data up to 1941 same as COBESST dataset. In addition to OI (Optimal Interpolation) scheme, this data set used an EOF reconstruction. The data provided by the NOAA/OAR/ESRL PSD, Boulder, Colorado, USA, from their Web site at http://www.esrl.noaa.gov/psd/.

The HadISST dataset includes an interpolated 1°x1° SST and a sea ice concentration over 1871-present. A reduced space optimal interpolation was used based on several sources: the Marine Data Bank (mainly ship tracks) SSTs, ICOADS up to 1981, and SSTs from satellites over 1982-present. The bucket correction process was applied to the data up to 1941 same as other data sets. The data provided from their Web site at http://www.metoffice.gov.uk/hadobs/hadisst/data/download.html.

Each data was trimmed as three different regions: a global domain (no trim), the NWP domain (N25°-55° and E110°-160°), and the KP area. Before conducting the CSEOF decomposition, these data sets were treated as follows. 1) The mean values for each grid point were removed to prevent those values to have a significant influence on CSEOFs. 2) The data were weighted by the square root of the cosine of latitude to consider the actual area of each grid. 3) Any grid points that were not continuous in time were removed. Like the satellite dataset, the annual signal of SST data was not removed.

3.5 Wind

PCTs of CSEOFs based on wind data play a role as a predictor (or independent) variable in multiple regression. A reanalyzed wind dataset applied to this research because of the same reason of SST case. In this study, the wind data from Twentieth Century Reanalysis Project Version 2 (hereafter NOAA-CIRES-WND) (Compo et al., 2006; Compo et al., 2011; Whitaker et al., 2004) was used. For this project, three pressure data sets were assimilated every six hours. The three data sets followed: ICOADS (Woodruff et al., 2011), ISPDv2 (International Surface Pressure Databank version 2) (Yin et al., 2008), and the International Best Track Archive for Climatic Stewardship (IBTrACS), (Knapp et al., 2010).

This model provided several outputs such as humidity, pressure for several layers, air temperature, horizontal wind speed, vertical wind speed and so on. Among them, two wind data sets were used in this study. These data sets have a 2° × 2° grid resolution and its time coverage is from 1851 to present. The data was trimmed as a box (N0°-60° and E100°-180°). Before conducting the CSEOF decomposition, these trimmed data sets were treated as follows; mean values for each grid point were removed because of the same reason of SST case; the data were weighted same as SST; Any grid points which were not continuous in time were removed. Like the satellite dataset, the annual signal was not removed.

The wind dataset provided by the NOAA/OAR/ESRL PSD, Boulder, Colorado, USA, from their Web site at http://www.esrl.noaa.gov/psd/.

3.6 Reconstructed sea level

Two sets of reconstructed sea level were used in this study. One provided long-term background trend, and the other was used for a validation purpose.

Church and White (2006 and 2011) provided a reconstruction from 1870 to 2009 using EOFs of SLA from satellite altimeter over 1993-2009. They applied the Reduced Space Optimal Interpolation technique. According to their research, the GMSL rose about 210 mm over 1880-2009, and the linear trend through 1900-2009 was 1.7 ± 0.2 mm per year. The resulting SLA is one of the most comprehensive and widely cited reconstruction results (Hamlington et al., 2012a). This data set was employed for long-term background trend for this study. This reconstruction has been extending to recent time, and the dataset has been available in public (http://www.cmar.csiro.au/sealevel/GMSL_SG_2011_up.html). However, this data contains the GMSL only; the spatial pattern is not concluded.

To create the reconstructed sea level anomaly, Hamlington et al. (2011) combined the CSEOFs of the satellite altimetry and historical TG record. This approach provides an advantage for describing local variations such as ENSO and PDO. This weekly analysis has a 1° × 1° grid resolution and its time coverage is over 1950- 2009. This data set was applied for the comparison with the reconstruction of this study. This reconstruction dataset can download from a Web site (ftp://podaac.jpl.nasa.gov/allData/recon_sea_level/preview/L4/tg_recon_sea_level/).

3.7. Ocean current data

A reanalyzed ocean current data from the NCEP (National Centers for Environmental Prediction) Climate Forecast System (CFS) was applied to verify the analysis results of a sea level change around the Korean Peninsula based on the GRACE Mascon data and the AVISO sea level anomaly data.

The NCEP Climate Forecast System Reanalysis (hereafter NCEP-CFSR) is a global, high-resolution (one-half of a degree; about 56 km), considering the interaction between atmosphere, ocean, land, and surface sea ice. The time coverage of this model is from January 1979 to March 2011.

A reanalysis data from the NCEP (National Centers for Environmental Prediction) Climate Forecast System (CFS) was applied to verify the analysis results of a sea level change around the Korean Peninsula based on the GRACE Mascon data.

The NCEP CFSR (Climate Forecast System Reanalysis) is most recent NCEP reanalysis having a global, high-resolution (one-half of a degree; about 56 km), considering the interaction between atmosphere, ocean, land, surface sea ice. The time coverage of this model is from January 1979 to March 2011 (Saha et al., 2010; Saha et al., 2014).

Among the various variables, e.g. each level atmospheric pressure, sea water temperature, air temperature, winds vector, ocean current vectors, surface temperature, the vertical ocean current speed at a depth of 5-meters and 15-meters (hereafter NCEP-CSFR-V05 and NCEP-CSFR-V15) were used for the verification. The current data sets were download from their website, https://www.ncdc.noaa.gov/.

3.8 Sea level fingerprints

Sea level fingerprints associating ice thickness in glaciers were used to estimate a partial SLR ratio from the continental water mass balance (Adhikari and Ivins, 2016; Farrell and Clark, 1976). This data is a linear SLR ratio for 1°× 1° grids using GRACE data over 2002-2015. According to Adhikari and Ivins (2016), a total mass change of the continental glaciers is about −530 Gt/yr and it raises the GMSL about 1.46 mm/yr. The sea level fingerprint maps resulted from different water sources: global noncryospheric terrestrial water storage, the Greenland ice sheet, Antarctic ice sheet, and all the rest glaciers are given as Figure **3**.**4**-Figure **3**.**7**.

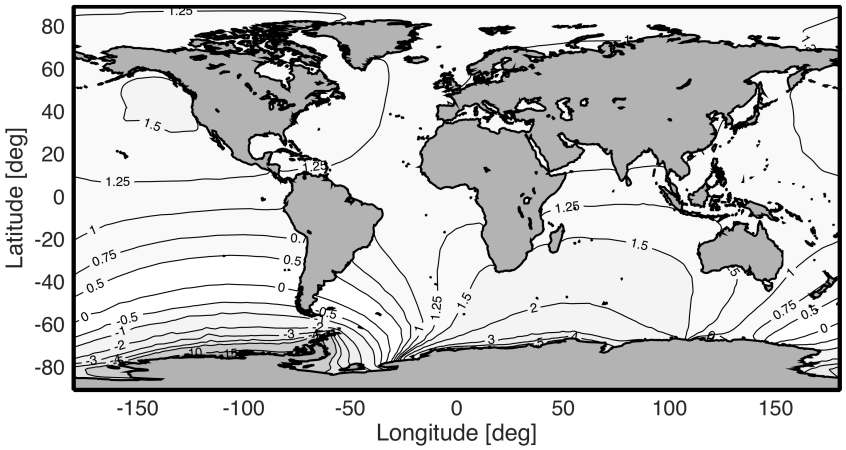

Figure 3.4. Fingerprint contour map corresponding to the mass change of Antarctic glaciers (normalized by global mean value)

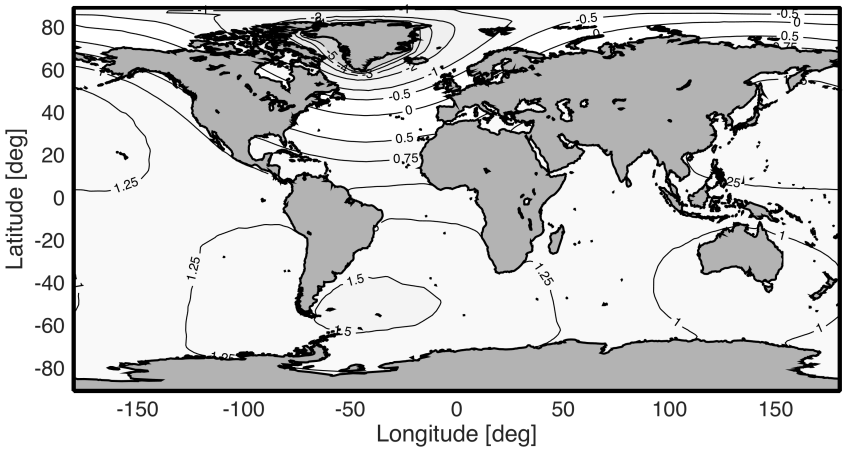

Figure 3.5. Fingerprint contour map corresponding to the mass change of Greenlandic glaciers (normalized by global mean value)

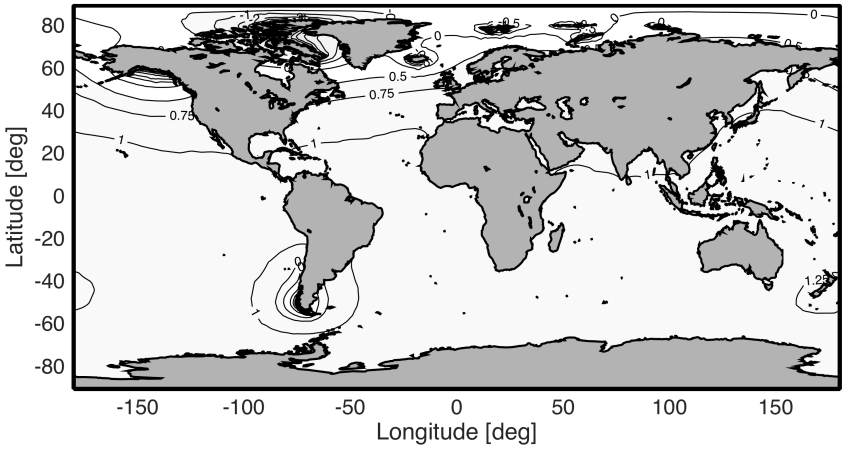

Figure 3.6. Fingerprint contour map corresponding to the mass change of glaciers without Greenland and Antarctic (normalized by global mean value)

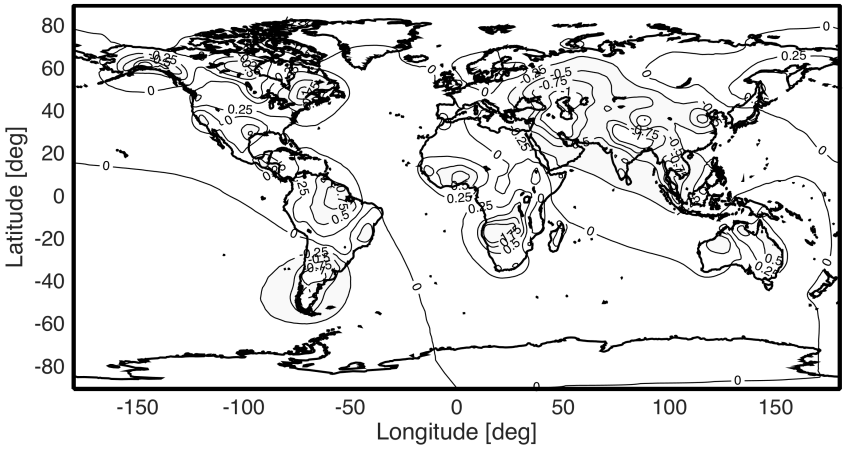

Figure 3.7. Fingerprint contour map corresponding to the change global noncryospheric terrestrial water storage

3.9 Projected global mean sea level

The GMSL scenarios under RCP scenarios are necessary to produce future sea level around the Korean Peninsula. In this study, we used the process-based model projections for each RCP scenario that was given in IPCC AR5's chapter 13 (Church et al., 2013). This data are the combining results of each sea level change source: thermal expansion, glaciers and ice-sheet melting, land water storage change, and possible ice-sheet rapid dynamics. This data set downloaded from their web site at http://www.ipcc.ch/report/ar5/wg1/.

This data is yearly averaged data with 90% confidence interval over 2006-2100. Hence it was interpolated to have monthly interval (see Figure **3**.**8** and Figure **3**.**9**).

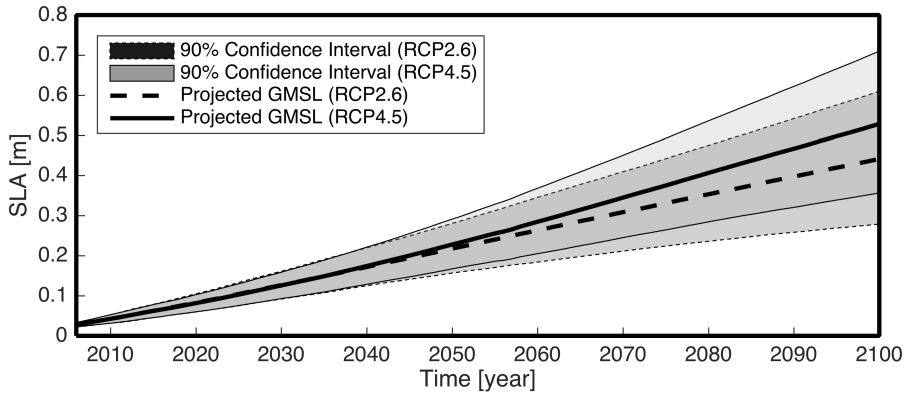

Figure 3.8. Projected global mean sea level of process-based models under RCP2.6 and 4.5

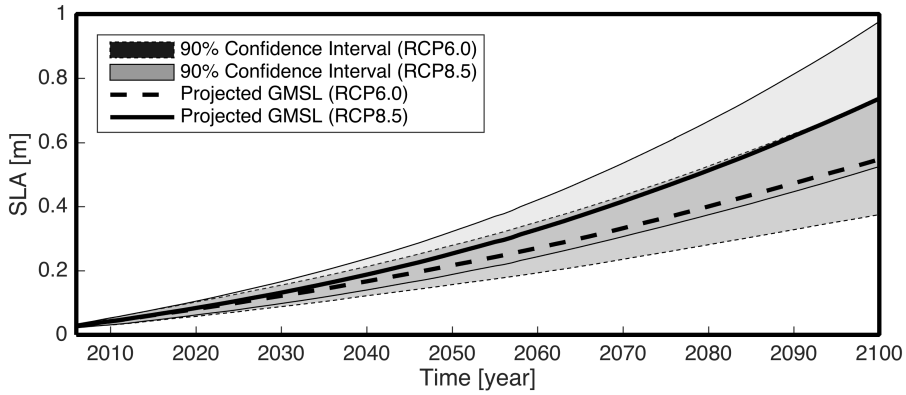

Figure 3.9. Projected global mean sea level of process-based models under RCP6.0 and 8.5

3.10 Future Sea Surface Temperature

For the prediction of the future SLA-KP, PCTs of CSEOFs based on future SST data play a role as a predictor (or independent) variable in a multiple regression. This study applied the SST of HadGEM2-ES (Collins et al., 2008) model results of RCP scenarios.

HadGEM2-ES is a coupled Earth System Model of the Met Office Hadley Centre for the CMIP5 centennial simulations. The HadGEM2-ES climate model combines an atmospheric GCM, an ocean GCM, and an Earth system models.

Nearly thousand of simulation results are opened in public. Among the simulated results, SST simulation data with RCP scenario (ensemble: r1i1p1) were used for the projection process. The applied SST data has 1°×1° spatial resolution and one month time interval over 1859-2300. The data downloaded at https://pcmdi.llnl.gov/.

Chapter 4 Method

Most of the studies on the reconstruction of sea level have been done on a global scale (Church and White, 2006, 2011; Church et al., 2004; Hamlington et al., 2012a; Hamlington et al., 2011; Hay et al., 2015). In some parts of the world with sparse observations, however, the accuracy of reconstruction is relatively low. Hence to get more accurate results, a local scale study is necessary to give enough information for engineering and policy-making purposes. Because of a range of difficulties, however, only a few regional reconstructions existed (Calafat and Gomis, 2009; Calafat and Jordà, 2011; Hamlington et al., 2012b).

The main difficulties are the lack of historical observations and biased spatial distributions of the TG data. The regional reconstruction around the KP suffers from both of these problems. The longest TG record is from 1930, and most of the TG data is available only after mid-1960 and a few TG data are available in the northern area around the KP. If the previous reconstruction scheme is applied, then it is likely only possible to obtain reliable results from 1970.

A modified reconstruction method is proposed for an area having poor TG coverage. The approach is based on the CSEOF decomposition and multivariate regression while taking into account a time lag. In this section, the procedure of the proposed scheme and fundamental theories are shown.

4.1 Sea Level Anomaly around the KP

Before conducting the reconstruction, it is necessary to understand the characteristics of SLA-KP. Using monthly averaged AVISO-KP, GRACE-Mascon, TG-KP and a sea level fingerprint, the features of SLA-KP were estimated as follows: sea level rise patterns, sea level rise ratio from water and ice balance on the land, and driving forces of the seasonal sea level variation around the KP.

4.1.1 Linear trend of SLA-KP

A linear trend map of SLA-KP was calculated by using AVISO-KP and TGs-KP over 1993-2015. For the calculation, annual signals were removed from both data sets. Subsequently, for the TGs-KP, linear trends were calculated for their observation periods.

4.1.2 Sea level rise from the mass balance of water and ice

Using the fingerprint dataset of Adhikari and Ivins (2016), a local SLR around the KP was calculated by summing the sea level fingerprint maps resulted from different water sources: global noncryospheric terrestrial water storage, the Greenland ice sheet, Antarctic ice sheet, and all the rest glaciers. The data was interpolated as on the same grids with the AVISO-SLA and it was trimmed and masked to correspond to the AVISO-SLA. Each fingerprint map was then summed into one trend map.

4.1.3 Origin of sea level variation

There are many factors which cause variations in sea level: thermal expansion, salinity change, current, mass balance, and so on. By comparing the time series between the SLA and mass field, a dominant factor can be understood; e.g., assuming no mass sources, if the sea level shows relatively bigger variation than the mass time series, this means that the steric factors such as salinity change and thermal expansion are dominant factors. To compare GRACE-Mascon and AVISO-SLA, the AVISO data had to be treated because the GRACE data was created based on a Mascon where the gravity value was same (see Figure **4**.**1**) even though the resolution of the data is 1°×1°. The spatial means in each Mascon were calculated for the AVISO-SLA. The average values were compared with the corresponding GRACE-Mascon and the correlation coefficients for each Mascon were then calculated.

4.1.4 Current effect on the SLA

An ocean current effects on the mass balances in the Yellow Sea and the East/Japan Sea were estimated by analyzing NCEP-CSFR current and GRACE-Mascon for the two Seas. Using the NCEP-CSFR-V05 and NCEP-CSFR-V15, a mass-flux time series was calculated and the calculated mass-flux time series were used to estimate the mass-flux balances in each area. The two areas' mass-flux balances and mass balance were analyzed.

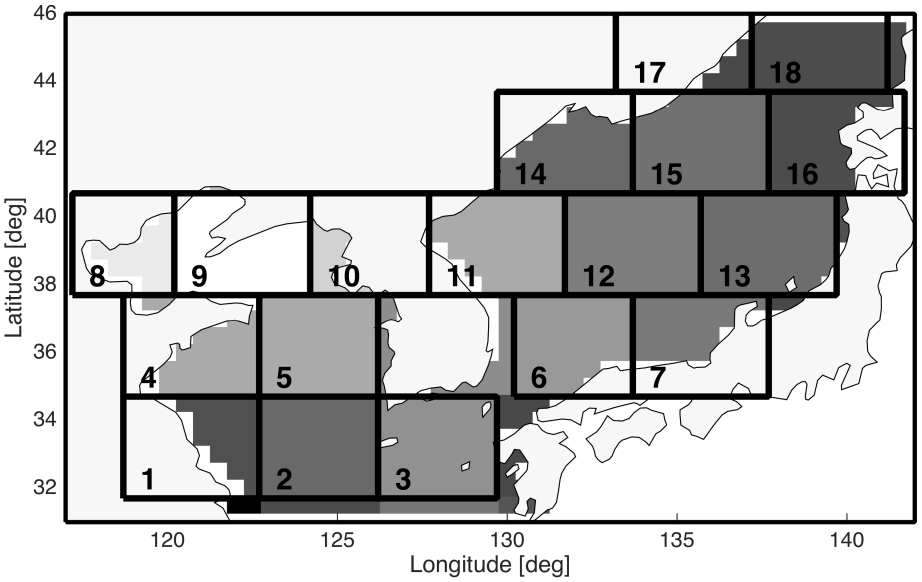

Figure 4.1. Location of each GRACE-Mascon (2002.05)

4.2 Cyclo-stationary Empirical Orthogonal Functions

To understand the complex response of a physical system, the decomposition of data regarding a set of basis functions is frequently applied. The decomposed basis functions give a better understanding of the sophisticated variability of the fundamental phenomenon. In practice, instead of finding a theoretical basis function, the empirical basis function is used because finding the theoretical basis function is very challenging and it requires a heavy computation. The simplest and most common computational basis functions are EOFs.

When a reconstruction selects the EOFs as basis functions, one basis function is defined as a single spatial map accompanied by a time series representing the amplitude modulation of this spatial pattern over a period. The assumption underlying EOF-based reconstruction is the stationarity of the EOF over the entire period. However the fact that many geophysical phenomena are cyclo-stationary is well known. That is, these processes are periodic over a certain inherent timescale, with the amplitude of this periodic process varying over time. Even though EOFs represent cyclo-stationary signals through a superposition of multiple modes, physically interpreting a combination of modes is difficult and often leads to errors. It also requires many EOFs to explain a relatively small amount of variability in a dataset.

To remedy some of these issues, Hamlington et al. (2011) introduced CSEOFs as a basis functions instead of EOFs. CSEOFs provide significant advantages over EOFs since CSEOFs can explain cyclo-stationary signals in one mode; this means the opportunity of separating physical signals into a single, easy-to-interpret mode (Kim et al., 2015; Kim and North, 1997; Kim et

al., 1996; Kim and Wu, 1999). Hamlington et al. (2011a, 2011b) showed CSEOFs provided significant benefits dealing with repeating signals such as ENSO (El Niño–Southern Oscillation) and MAC (Modulated Annual Cycle) signals.

Consider a simple system defined by the equation:

$$T(r,t) = \sum_i LV_i(r)PCT_i(t) \quad (1)$$

where $LV(r)$ is a physical process (or loading vector) modulated by a time series $PCT(t)$ (principal component time series or PC time series).

Combining each LV and PCT pair, a signal of single EOF mode can be produced. The SVD (Singular Value Decomposition) process calculates the LV and PCT. Theoretically, a summation of infinite modes Combining each LV and PCT pair, a signal of single EOF mode can be produced. The SVD (Singular Value Decomposition) process calculates the LV and PCT. Theoretically, a summation of infinite modes can represent the cyclo-stationary physical processes. However, like the claims that by Dommenget and Latif (2002), representing the cyclo-stationary signal with stationary EOFs can lead to an erroneous and ambiguous interpretation of the data.

The CSEOF analysis has been proposed and improved since 1996 to capture the cyclo-stationary patterns and longer scale fluctuations in geophysical data (Kim and Chung, 2001; Kim et al., 2015; Kim and North, 1997; Kim et al., 1996; Kim and Wu, 1999). The CSEOF analysis can capture the time varying signals as a single mode by giving a time dependency to the loading vectors,.

The system is defined as follow.

$$T(r,t) = \sum_i CSLV_i(r,t)PCT_i(t) \quad (2)$$

$$CSLV(r,t) = CSLV(r,t+d) \quad (3)$$

where $CSLV$ is a cyclo-stationary LV and it is time dependent and periodic with d (called as nested period).

In the condition that the space-time covariance function or matrix is periodic in time with the nested period d, the loading vector and corresponding PCT can be calculated by,

$$C(r,t;r',t')CSLV_i(r',t') = \lambda_i CSLV_i(r,t) \quad (4)$$

where r' is other points in space and t' represents other points in time and $C(r,t;r',t')$ is a spatiotemporal covariance function.

However, in equation (4) the covariance function is not a square matrix; this means the calculating of loading vectors and PCTs is not straightforward like the EOF's LVs and PCTs. To make the covariance matrix in equation (4) to be solvable, the original system $T(r,t)$ in equation (2) is Fourier transformed as below.

$$T(r,t) = \sum_{k=0}^{d-1} a_k(r,t)\exp(2\pi ikt/d) \quad (5)$$

Applying cyclo-stationary assumption of the original data, equation (5) is given as,

$$T(r,t) = \sum_{k=0}^{d-1}\sum_l a_{kl}(t)Y_l(r)\exp(2\pi ikt/d) \quad (6)$$

Now, the equation (4) is

$$C_F(t;t')u(t') = \lambda_i u(t) \tag{7}$$

where, $C_F(t;t')$ is a temporal covariance function in Fourier domain and $u(t)$ is an eigenfunction.

The estimated $u(t)$ value plays a role of estimation of the eigenfunction.

$$U(r,t) = \sum_{k=0}^{d-1} \sum_l u_{kl}(t) Y_l(r)\, exp(2\pi ikt/d) \tag{8}$$

The loading vector of the three-dimensional CSEOFs is given as

$$LV_n(r,t) = \exp(2\pi nt/N)\, U(r,t) \tag{9}$$

The PC time series can be calculated as follow.

$$PC(t) = u(t)a(t) \tag{10}$$

The studies of Kim et al. (1996), Kim et al. (1997) and Kim et al. (2015) provide more detailed walk-through for the CSEOF computation and properties.

4.3 Multivariate regression using CSEOFs

When considering the complete Earth climate system, one variable is often directly connected to another variable. In some cases they are impacted by a common physical process, or in other cases, one variable may directly influence another. To take advantage of these relationships and establish links, we can perform a multivariate linear regression.

The multivariate (or multiple) linear regression is an extension of the linear regression analysis that involves more than one independent variable. In general, a single geophysical signal is related to multiple variables. This system can be expressed as the response (or dependent variable) y is related to k regressor (or predictor or independent) variables x; the model can be written as below.

$$y = \beta_0 + \beta_1 x_1 + \beta_2 x_2 + \cdots + \beta_k x_k + \varepsilon \qquad (11)$$

The equation (11) is called a multiple (multivariate) linear regression model with k regressors. The β_0, β_1, β_2, $\cdots$, β_k are regression coefficients and the ε is random error.

A multiple linear regression model is frequently used as empirical models or approximating functions. If the real relationship between y and $x_1, x_2, \cdots, x_k$ is unknown, but it is over specified ranges of the regressor variables, the multivariate linear regression model can be a good approximation to the actual relationship. The ordinary least squares (OLS) estimation is applied to find regression coefficient based on the known or observed dataset. The multivariate linear regression is a popular approach to predict the geophysical signals. For more details of this method, one can refer to the previous studies such as Montgomery et al. (2015).

In this study, the response variables are each PCT of AVISO-KP's CSEOF and the predictor variables are all PCT of each SST dataset's CSEOF. The equation (11) can be written as below.

$$PCT_{SLA}^{i} = \beta_0 + \beta_1 PCT_{SST}^{1} + \beta_2 PCT_{SST}^{2} + \cdots + \beta_k PCT_{SST}^{k} + \varepsilon \qquad (12)$$

where PCT_{SLA}^{i} is the i-th PCT of SLA-KP's CSEOF, PCT_{SST}^{i} is the i-th PCT of SST's CSEOF.

The matrix form of the equation (12) is:

$$\begin{bmatrix} T_1^i \\ T_2^i \\ \vdots \\ T_n^i \end{bmatrix} = \begin{bmatrix} 1 & P_1^1 & P_1^2 & \cdots & P_1^k \\ 1 & P_2^1 & P_2^2 & \cdots & P_2^k \\ \vdots & \vdots & \vdots & \ddots & \vdots \\ 1 & P_n^1 & P_n^2 & \cdots & P_n^k \end{bmatrix} \begin{bmatrix} \beta_0 \\ \beta_1 \\ \vdots \\ \beta_k \end{bmatrix} + \varepsilon \qquad (13)$$

where T_n^i is the n-th PCT_{SLA}^{i} and P_n^k is the n-th PCT_{SST}^{k}. In equation (13), let the response matrix is y and the predictor matrix is X and the coefficient matrix is β then the least-squares estimator of β is calculated by follow.

$$\hat{\beta} = (X'X)^{-1}Xy \qquad (14)$$

Commonly, many geophysical signals have lagged relations with other geophysical signals (Bojariu and Gimeno, 2003; Dettinger et al., 1998; Hamlet et al., 2005; Hendon et al., 2007; Kawamura et al., 2004; McPhaden et al., 2006; Redmond and Koch, 1991). To check the lagged relations between the PC time series of SLA and SST, the normalized cross-correlation between PCTs was calculated using MATLAB function; based on the MATLAB help documentary for Econometrics Toolbox (Box et al., 2015; LeSage, 2010) the process can be written as follow.

The normalized cross-correlation is an estimate of the covariance between two time series, $x_1(t)$, and $x_2(t)$, at lags $k = 0, \pm 1, \pm 2, \cdots$.

The estimate of the lag k cross-covariance is

$$C_{x_1x_2}(k) = \begin{cases} \frac{1}{T}\sum_{t=1}^{T-k}[x_1(t)-\bar{x}_1][x_2(t+k)-\bar{x}_2]; & k = 0,1,2,\ldots \\ \frac{1}{T}\sum_{t=1}^{T+k}[x_2(t)-\bar{x}_2][x_1(t-k)-\bar{x}_1]; & k = 0,-1,-2,\ldots \end{cases} \quad (15)$$

where $\bar{x}_1$ and $\bar{x}_2$ are sample means of each time series. Then the normalized cross-correlation is

$$\rho_{x_1x_2}(k) = c_{x_1x_2}(k)/\sigma_{x_1}\sigma_{x_2} \quad (16)$$

where σ_{x_1} and σ_{x_2} are sample standard deviations.

Two random variables can be considered to be statistically uncorrelated if the magnitude of the correlation coefficient is less than 0.3; they can be deemed to have perfect correlation if the absolute value of the correlation coefficient is greater than 0.9 (Mahadevan and Haldar, 2000). Before performing the multivariate linear regression system like equation (12), the cross-correlation was calculated using equations (15) and (16). The dependent modes were selected based on their cross-correlation values (bigger than 0.4) and using the selected mode the multiple linear regression system was established.

By assuming the lag of the n-th mode having maximum cross-correlation as ρ_n, the i-th mode's PCT of AVISO-KP can be given as follow based on the equation (12).

$$PCT^i_{SLA}(t) = \beta_0 + \sum_{n=1}^{m}\beta_n PCT^n_{SST}(t-\rho_n) + \varepsilon. \quad (17)$$

4.4 Reconstruction of the past SLA-KP

Using the CSEOFs of AVISO -KP over 1993-2015, the past SLA-KP was reconstructed. In this section, the general explanation of this scheme is provided.

By extending the PCT of AVISO-KP's CSEOFs, we can rebuild the past SLA. A unique characteristic of this reconstruction with others is the nonuse of the local TG data sets. Instead of applying the local TG data, the GMSL was used as the essential mean variation in the region.

The difference between GMSL and regional MSL (Mean Sea Level) was calculated to estimate the average SLA-KP. The second mode of AVISO-KP's CSEOF represents the mean sea level change around the KP well. Hence, after removing GMSL from the AVISO-KP at each grid point, the CSEOF decomposition was conducted. The second mode of the CSEOF decomposition represents the difference between GMSL and AVISO-KP. This means that if we conduct the reconstruction using AVISO-KP that has no GMSL (hereafter AVISO-KP0), then the reconstructed SLA-KP includes no GMSL, too.

Using the regression coefficients and lagged relationship between the PCTs of each SST dataset and AVISO-KP0, we can extend the PCTs of AVISO-KP0 through equation (17). By combining the LVs of AVISO-KP0 and extended PCTs, we can rebuild the past SLA-KP with no GMSL.

Finally, after adding up the GMSL to the reconstructed SLA-KP with no GMSL, the SLA-KP can be reconstructed with a regional mean sea level change.

4.5 Estimate of confidence intervals

To estimate the confidence intervals of the reconstructions in this study, both AVISO-KP and the SST reanalysis data are assumed as correct values. Based on the assumption, the multiple linear regression provides confidence intervals for the regression coefficient. The GMSL of Church and White (2011) which played the role of the long-term background change of the SLA-KP also provides their confidence interval.

A MC (Monte Carlo) simulation was carried out using the confidence intervals of multiple linear regression coefficients and GMSL. The MC simulation created 1000 sample-sets for each SLA-KP reconstruction. Using the sample-sets, the confidence intervals of each reconstruction were calculated. The confidence intervals of ensemble mean of all reconstructions sample-sets were also calculated.

4.6 Sea Level Reconstruction Process

A procedure of the current reconstruction is given by the following.

1) The necessary data sets were collected. All data sets that were used in this study were available in public (see Chapter 3). Every dataset, except the AVISO-SLA, was treated to have the time span of 1891-2014. The AVISO-SLA was trimmed to containing the ocean around the KP only (N31°-46° and E117°-142°). The southeast region of the Japanese islands was removed. Every SST dataset was cut into three regions: around the KP (same box with AVISO-KP; hereafter add '-KP'), the Northwest Pacific Ocean (N25°-55° and E110°-160°; hereafter add '-NWP'), and global (no trimming). The wind data was trimmed as a box (N0°-60° and E100°-180°). All grid points that were not continuous in time were removed for every dataset. We prepared fourteen data sets: AVISO-KP for regression target, thirteen data sets for regression predictors.

2) GMSL and mean values were removed from AVISO-KP at each grid point. Each dataset was weighted by the square root of the cosine of latitude to consider the actual area of each grid.

3) The CSEOF decomposition was applied to all data sets (AVISO-KP, SST data sets, and wind dataset) with twelve months nested period.

4) The lagged relation between PCTs of AVISO-KP and PCTs of each SST dataset were estimated with two years maximum lagging boundary.

5) Using the PCTs of each dataset's CSEOF, the multiple linear regression systems were built based on the equation (17) over 1993-2014. In this regression, the target variables were each PCT of AVISO-KP and the predictors are PCTs of each SST data sets. The regression coefficients and their confidence intervals were estimated to extend target variables.

6) Applying MC simulation that used the confidence intervals of regression coefficients, we randomly generated a thousand sample-sets of each extended PCT of AVISO-KP.

7) By combining the extended PCTs to the LVs of AVISO-KP, we can produce a thousand reconstructed SLA-KP0s. By adding up the randomly generated GMSL to the SLA_KP0, a thousand of SLA-KPs were reconstructed.

8) Finally, by statistical analysis of each time step of the random samples, we can estimate the mean variation and their confidence intervals of each reconstruction.

4.7 Validation of the reconstruction

The reference data sets were not enough for verifying the current reconstructions. Especially, before 1970, only a few TG records are available, and there is no TG data at all before 1930. For comparison purposes, in addition to the TGs-KP, we used the reconstructed data set of Hamlington et al. (2011). Their reconstruction was based on the TG records and satellite altimetry's CSEOF. The reconstruction results over 1970-2009 are quite reliable, because, after 1970, the number of available TG data sets around the KP is enough to guarantee the reconstruction results.

The correlation coefficients and NRMSE (Normalized Root Mean Square Error) values for the entire domain and each TG location are calculated.

By comparing these two values, we decided the best reconstruction case among the thirteen reconstructions.

4.8 Sea Level Projection under RCP scenarios

The reconstruction scheme that was introduced in previous sections has a simple structure. Firstly, the CSEOF decomposed satellite data were extended into the past to rebuild the sea level spatial patterns that have no GMSL. These spatial patterns, of course, have time-dependent variations but those fluctuations are independent of GMSL because the GMSL values were removed before the CSEOF decomposition as explained in previous sections. Next, the GMSL was combined into the reconstructed spatial pattern. Then, we can get the reconstructed sea level. We can produce various kind of sea level by replacing the GMSL.

Using the simple structure of the reconstruction process, we can conduct the projection of future sea levels around the KP. The major different things follow:

1) In sea level projection, the PCTs of satellite data are extended to the future and are then applied to the corresponding spatial patterns. The reconstruction process applied regression analysis considers lagged relationship to extend the PCTs to the past. In the reconstructing process, SST's PCTs played a role of predictors. However, for the projection process, we applied future SST data from CMIP5 AOGCM model as predictors. Fundamentally, even the CMIP5 AOGCM models produced SST and sea surface height; their outputs are not real values but only they are based on the similar environment. Therefore, we cannot establish the relationship between observed satellite altimeter data and CMIP5 models' output. By considering lagged relationship, however, we

can overcome this problem, because the regression process of this study only used high correlated predictor variables considering lagged relationship.

2) The projected GMSL replaced the observed GMSL. Through combining the projected GMSL under RCP scenarios, we can give trends to the spatial patterns generated prior step. The CSEOF LVs and PCTs include information about the difference between the GMSL and regional sea levels. Base on the idea that the local sea level variations have been loaded on the GMSL, we assume that the concept is going to be valid for the future. Starting from above assumptions, we can draw a conclusion that if we can extend the PCTs of satellite altimeter to the future, we can make a reasonable projection of the future sea level variation; which is loaded on the GMSL.

The PCT extension process is given in follows:

1) Conducting CSEOF decomposition of satellite altimeter data and projected SST data in the same way in the reconstruction.
2) Carrying out CSEOF regressions after the same method of the reconstruction process.
3) Extending AVISO's PCT into Future using the established regression coefficient.
4) Combining AVISO's CSLV and the extended PCT.

Then the projected GMSLs under RCP scenarios, which were introduced in IPCC AR5, are connected to the predicted spatial variation in the previous step. This process is exactly same with the reconstruction.

Chapter 5 Results

5.1 Sea Level Anomaly around the KP

5.1.1 Sea level anomaly from satellite altimeter

Using AVISO-KP over 1993-2015, a linear trend map was estimated as shown in Figure **5**.**1**. The mean trend in the region was found to be 3.1 ± 0.5 mm/yr. This SLA pattern is very close to the global SLA trend, 3.0 ± 0.0 mm/yr (see Figure **5**.**2**). Most of SLA-KP trends were close to the mean, but some part of the East/Japan Sea and close area to the land of the Yellow Sea showed extreme trends. The North East and the Southern areas showed relatively consistent trends with the mean value.

5.1.2 Sea level anomaly from TGs-KP

The linear trends of SLA using the TGs-KP and corresponding AVISO-SLA points are shown in Figure **5**.**3** and Figure **5**.**4**. A mean SLA (hereafter MSLA) trend of the TGs-KP is 4.31 mm/yr and this value is about 40 % higher than the MSLA trend of the corresponding AVISO-SLA points. Assuming the AVISO-SLA is a reference data, 5 TGs (about 10% of overall TGs-KP) showed less than 30% error (see Figure **5**.**5**).

Correlation coefficients between TGs-KP and corresponding AVISO-KP points were calculated for two cases: with seasonal signals, and without seasonal signals (see Figure **5**.**6** and Figure **5**.**7**). With the annual signals the average correlation coefficient is about 0.89 and without the seasonal signals it was about 0.48.

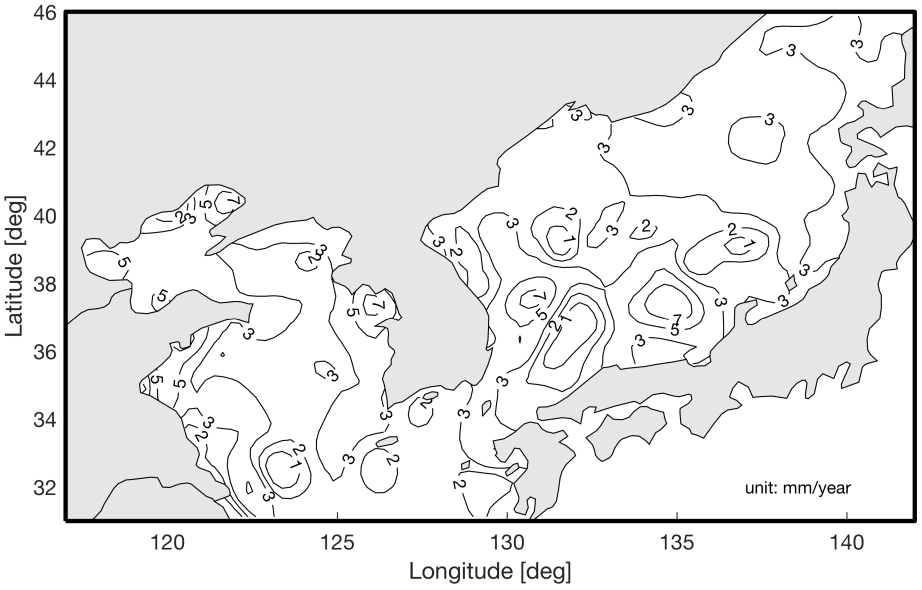

Figure 5.1. Linear trend map of SLA-KP

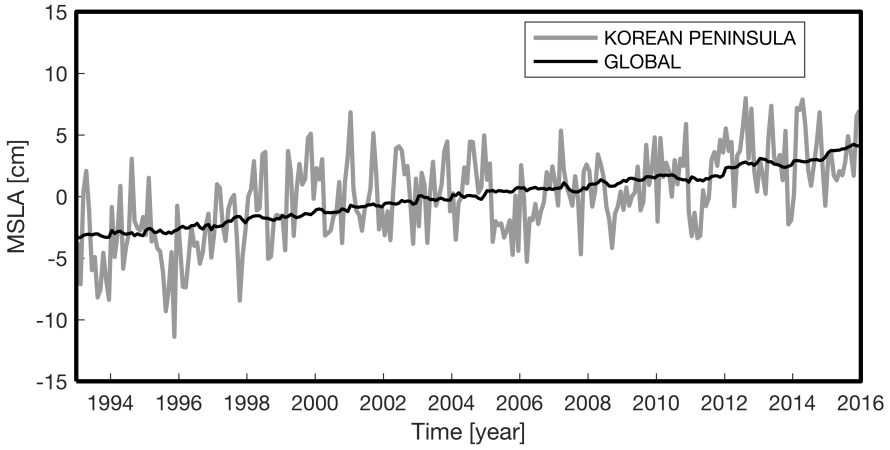

Figure 5.2. Spatial mean SLA time series around the KP over 1993-2015

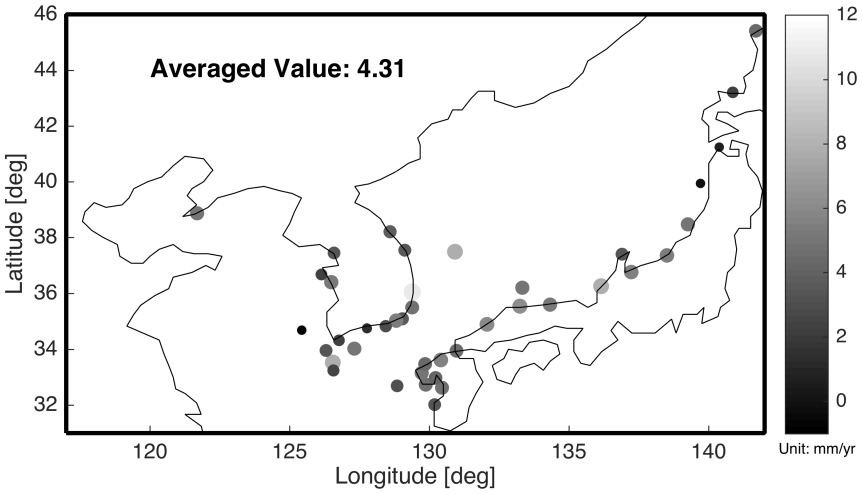

Figure 5.3. SLA linear trends over 1993-2013 using TGs-KP

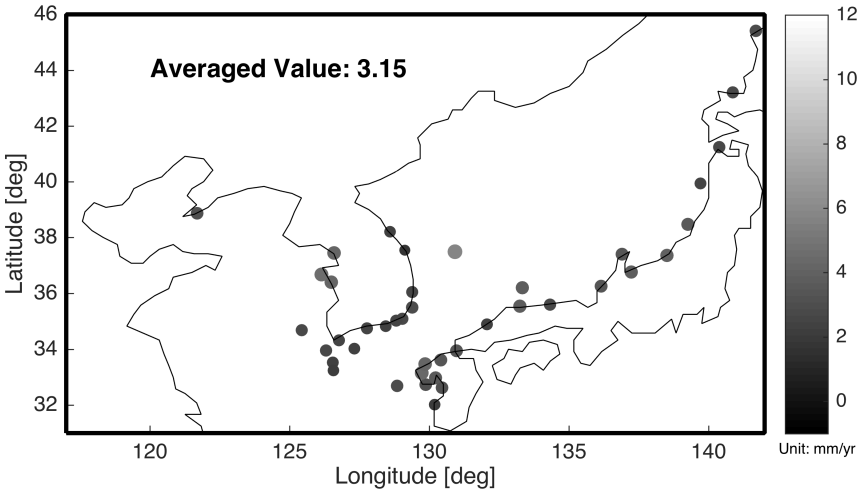

Figure 5.4. SLA linear trends over 1993-2013 using AVISO-SLA

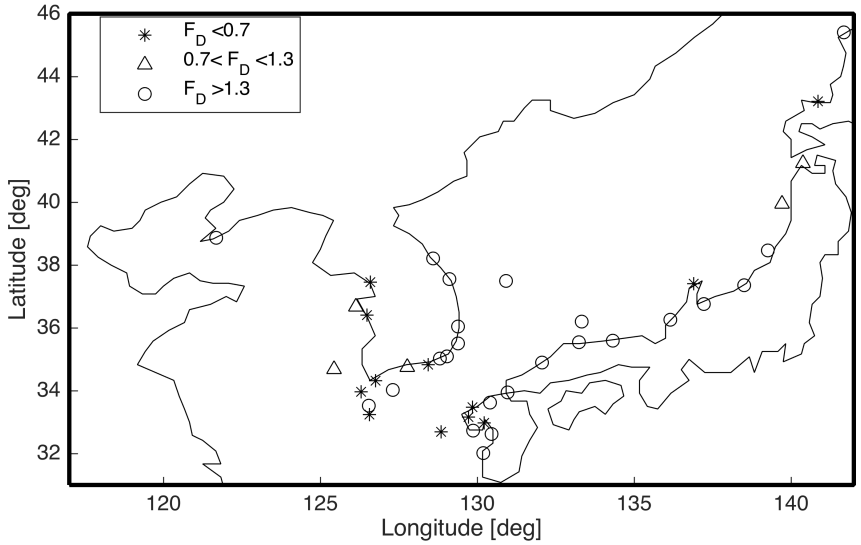

Figure 5.5. Comparison SLA linear trends between TGs-KP and AVISO-SLA over 1993-2013; **F_D** is normalized TGs-KP linear trend value with AVISO-SLA linear trend

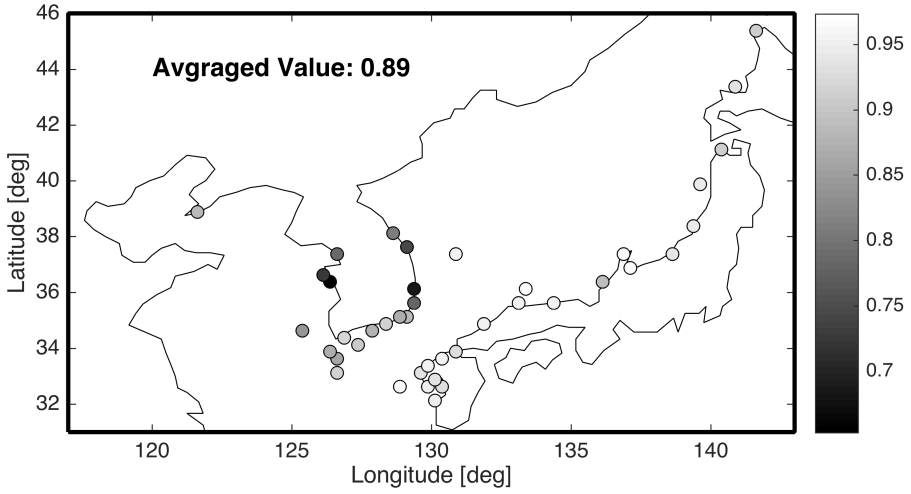

Figure 5.6. Correlation Coefficients between TGs-KP and AVISO-SLA points with seasonal signals

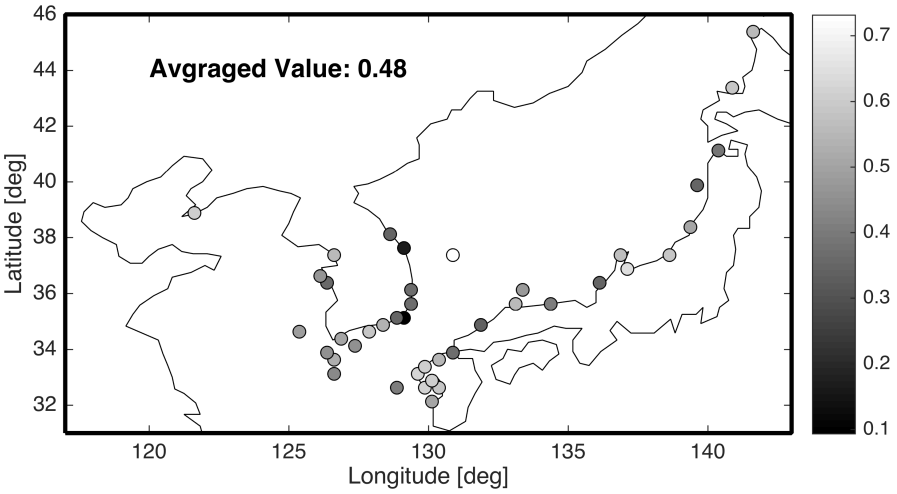

Figure 5.7. Correlation Coefficients between TGs-KP and AVISO-SLA points without seasonal signals

5.1.3 Gravity field anomaly around the KP

Using the GRACE-Mascon data, a mass balance around the KP was estimated in each Mascon. Resulting data was compared with the sea level in the corresponding location in terms of correlation coefficients (ρ_{GA}) between GRACE-Mascon and AVISO-SLA for each Mascon of GRACE data. Using calculated ρ_{GA}^{i} (here i represents zone) values, the entire area was divided into four regions, see Figure **5.8**. The ρ_{GA}^{i} values for each zone are ρ_{GA}^{I} = 0.87, ρ_{GA}^{II} = 0.60, $\rho_{GA}^{III} = 0.10$, and $\rho_{GA}^{IV} = -0.10$. This means that the SLA of the Western and Southern Seas around the KP is highly correlated with the gravity field.

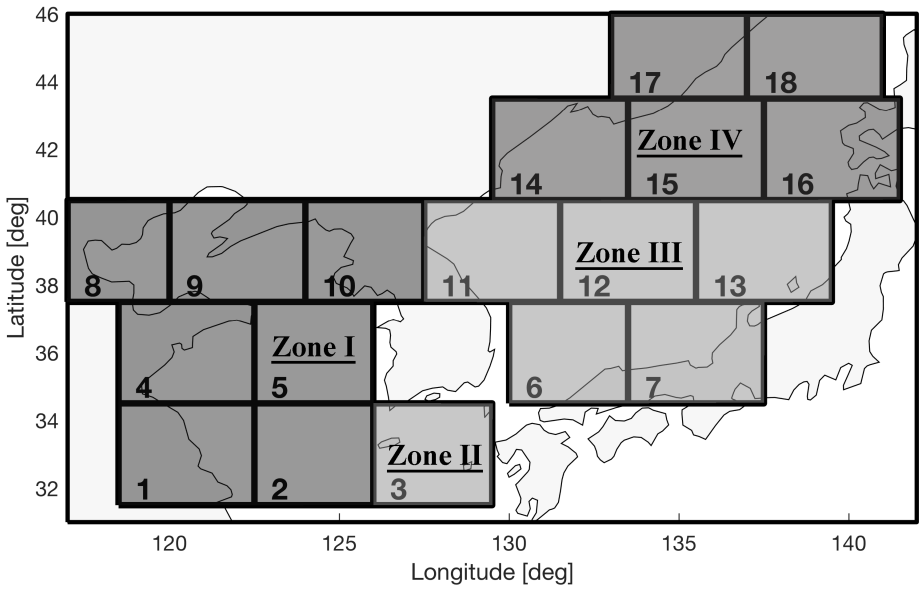

Figure 5.8. Zone division with respecting to correlation coefficients between GRACE-Mascon and AVISO

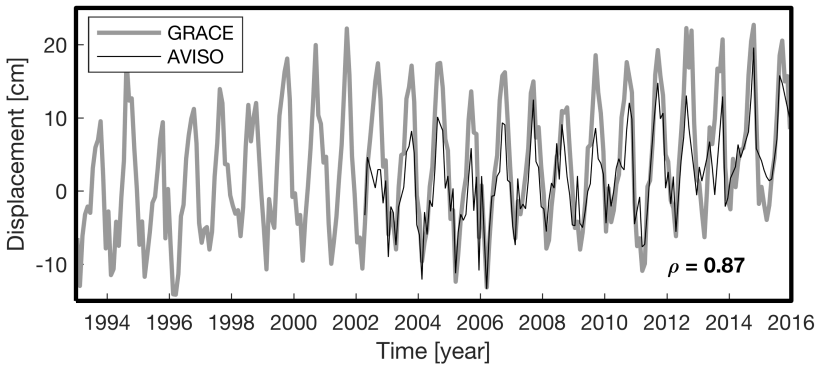

Figure 5.9. Comparison between the mean sea level from AVISO and a mean gravity field from GRACE for Zone I

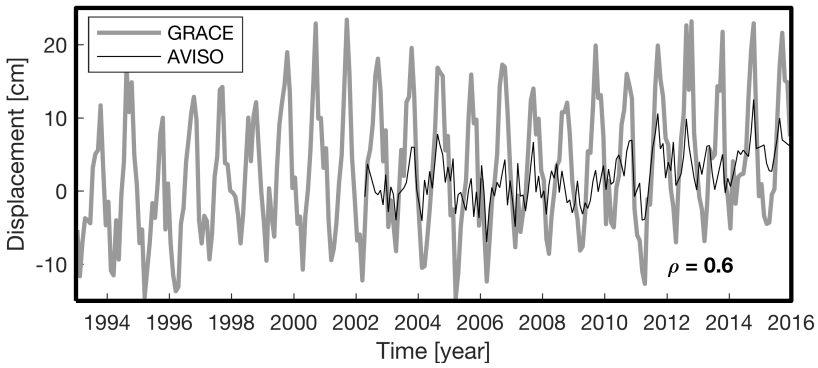

Figure 5.10. Comparison between the mean sea level from AVISO and a mean gravity field from GRACE for Zone II

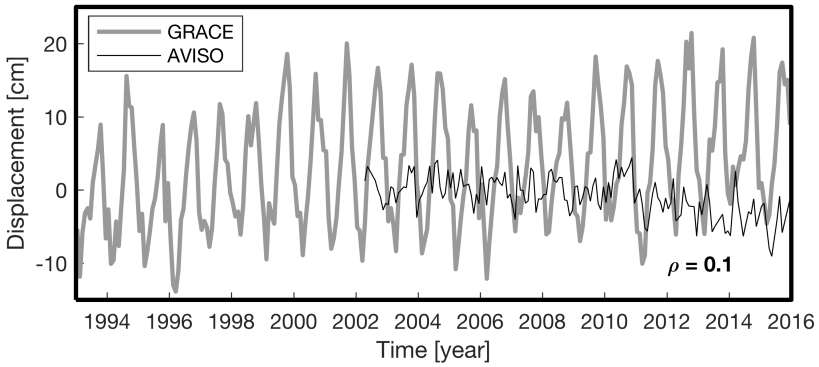

Figure 5.11. Comparison between the mean sea level from AVISO and a mean gravity field from GRACE for Zone III

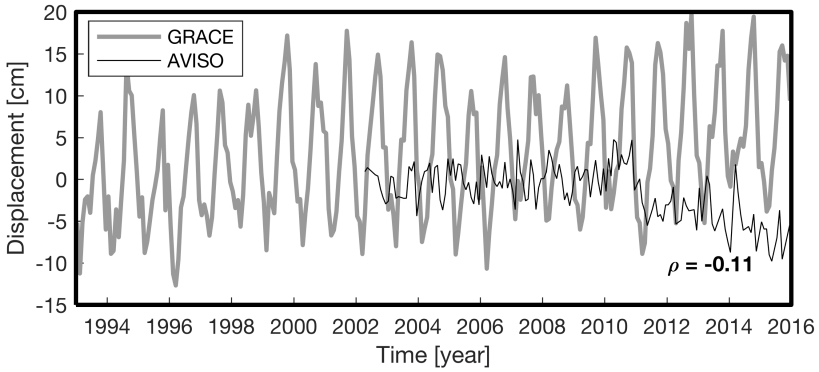

Figure 5.12. Comparison between the mean sea level from AVISO and a mean gravity field from GRACE for Zone IV

To understand the different correlations between the GRACE-Mascon and AVISO-SLA, the current reanalysis data of NCEP-CFSR was applied. The balances of current velocity at each boundary were calculated at three different boundaries (West: E129.2-137, N34.7; South East: E129.2-137.7, N35.7; North East: E133.2-141.2, N43.7). The balances of mass flux are given in Figure 5.13.

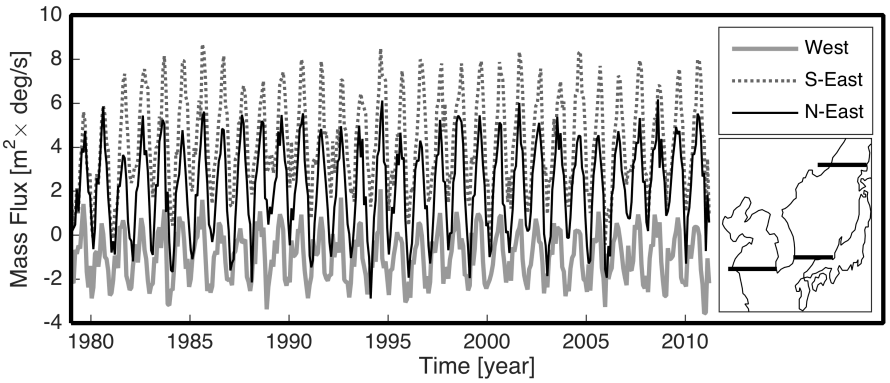

Figure 5.13. Mass flux near the surface area (< 15m) over the boundaries: West (E118.5-126.5 & N34.7), South East (E129.2-137.7 & N35.7), and North East (E133.2-141.2 & N43.7).

Using the velocity values at 5 and 15 m depth, the areal mass flux balances were calculated to figure out their effect on sea level. For the Yellow Sea, the flux balance at the boundary is directly related to the mass balance because the Yellow Sea is surrounded by land. For the East/Japan Sea area, however, the mass fluxes can come in or out through the both boundaries. The areal flux balance for the East/Japan Sea was estimated by subtracting the mass flux in the northern boundary from the southern boundary. The resulting areal mass flux balances are given in Figure 5.14. The balance of mass fluxes shows that the current effect on the sea level anomaly is the reverse of each other.

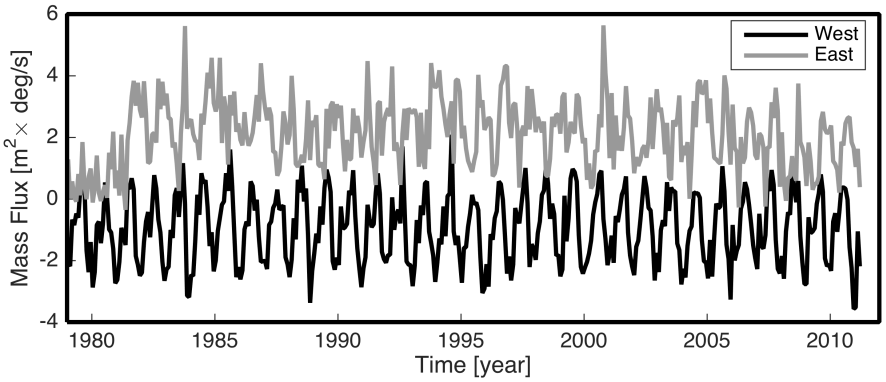

Figure 5.14. Mass flux balances near the surface area (< 15m) over the domains: West and East ($F_{SE} - F_{NE}$ where F_{SE}= mass flux over South East and F_{NE}= mass flux over North East; see Figure 5.13).

5.1.4 Sea level change due to the change of continental water mass

Using each fingerprint map, the SLR ratios around the KP were given as follows: 0.25 mm/yr, 1.01 mm/yr, 0.41 mm/yr, and 0.01 mm/yr for Antarctic Ice Sheet, Greenland Ice Sheet, glaciers except for the previous two regions, and the global noncryospheric terrestrial water storage, respectively. By adding up the fingerprint maps caused by different glacial sources, an overall fingerprint map around the KP was created as shown in Figure **5**.**15**. The spatial mean considering areal weight according to different latitudes was 1.76 mm/yr.

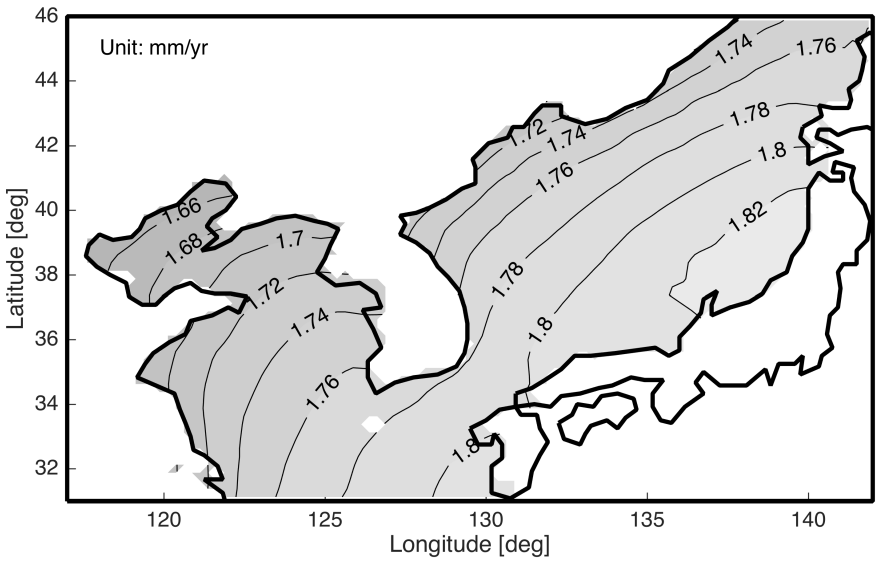

Figure 5.15. Linear sea level change ratio map caused by Antarctic Ice Sheet, Greenland Ice Sheet, glaciers but previous two regions, and Terrestrial water storages.

5.1.5 CSEOF Analysis of SLA-KP

Applying CSEOF analysis scheme (Kim et al., 2015; Kim and North, 1997; Kim et al., 1996), AVISO- KP was decomposed into Loading Vectors (LVs) and resulting time series of Principle component (PCTs). Twenty-nine modes were used to explain 99.9 % of the variance of the SLA around the KP. The decomposed modes were ordered with the dominant mode given first and a cumulative variance for each mode is given in Figure **5**.**16**. The first four modes' LVs and PCTs, which explain about 80 % of total variation, are given in Figure **5**.**17** - Figure 5.20.

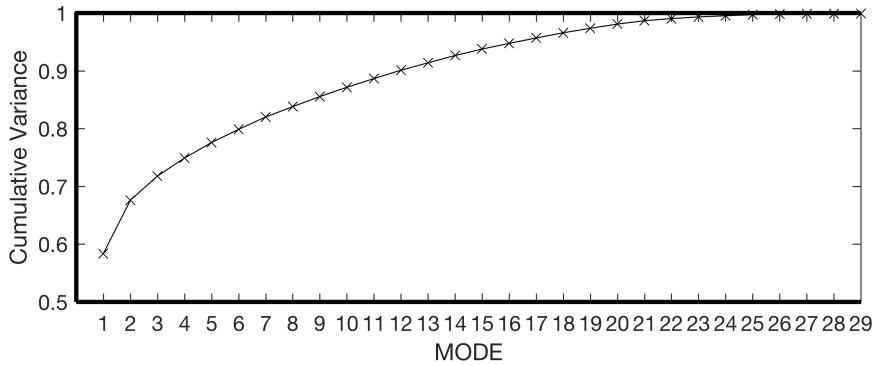

Figure 5.16. Cumulative variance of each mode of CSEOF analysis of AVISO-KP

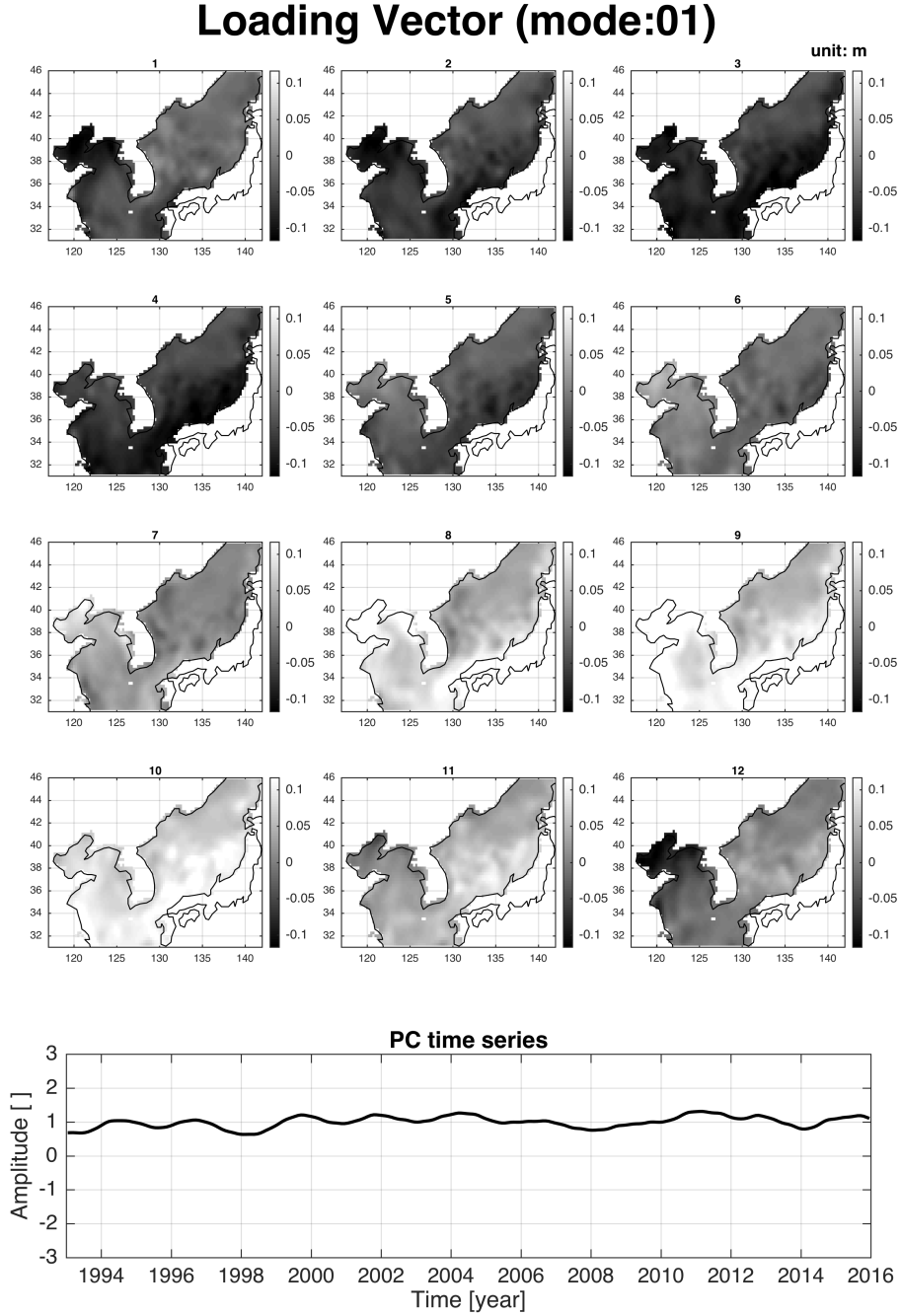

Figure 5.17. 1st mode's Loading Vector and PC time series of CSEOF Analysis for AVISO-KP

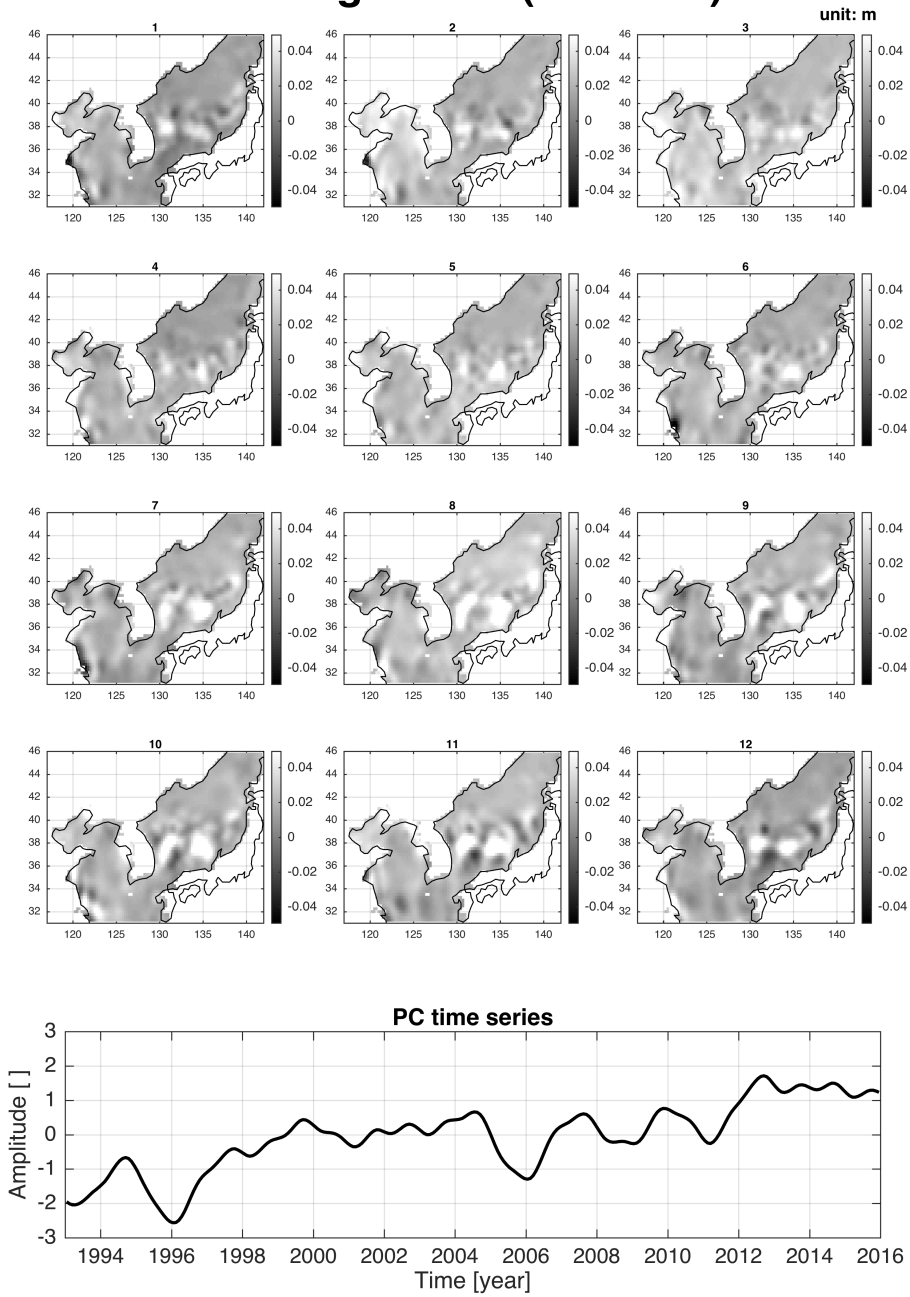

Figure 5.18. 2nd mode's Loading Vector and PC time series of CSEOF Analysis for AVISO-KP

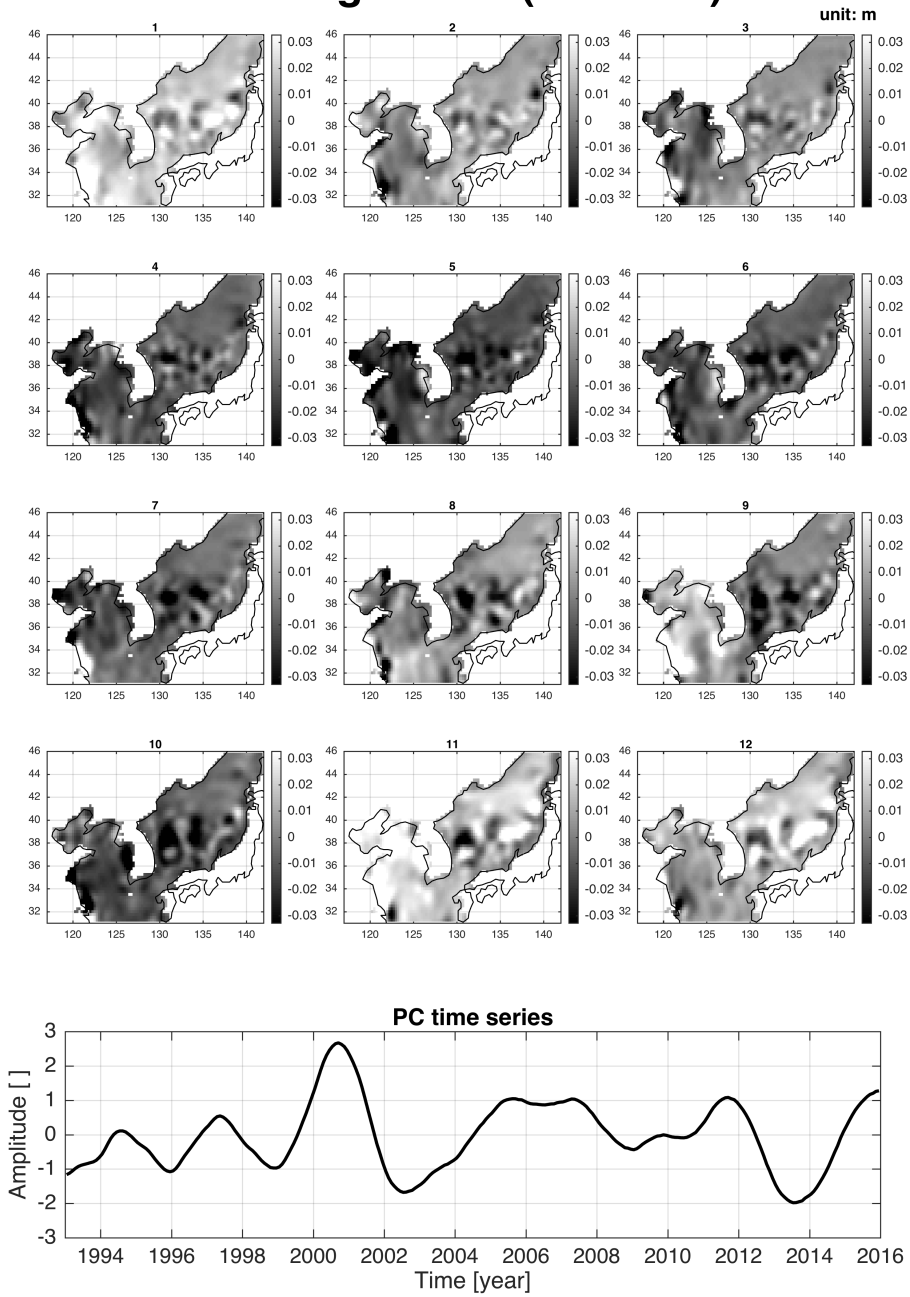

Figure 5.19. 3rd mode's Loading Vector and PC time series of CSEOF Analysis for AVISO-KP

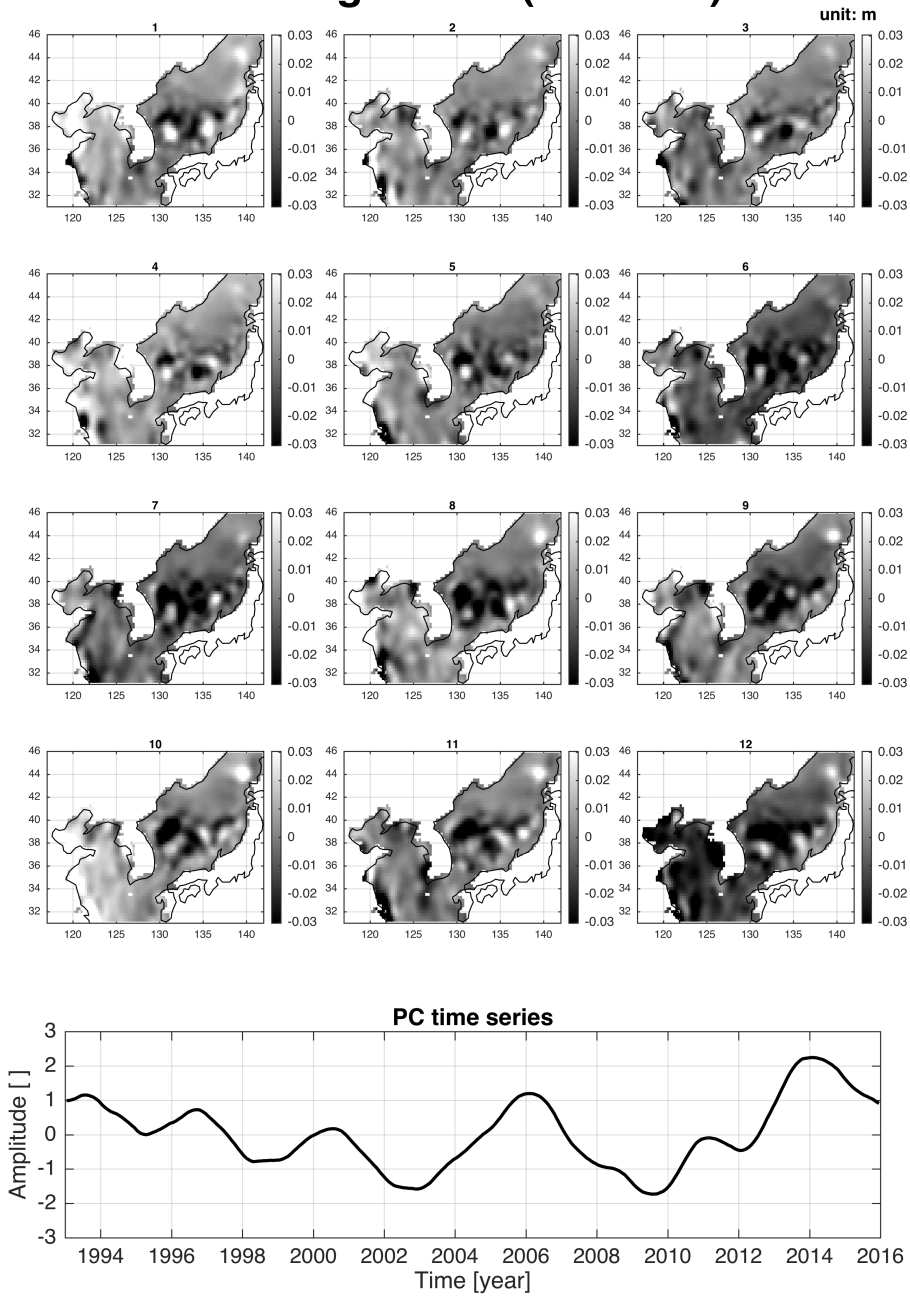

Figure 5.20. 4th mode's Loading Vector and PC time series of CSEOF Analysis for AVISO- KP

Each decomposed mode can be recast by multiplying each LV by the corresponding PCTs. Every mode was then reassembled. The first four modes' reconstructions are given in Figure 5.21. To estimate each mode's effect on sea level, a linear trend of each mode's SLA was calculated as shown in Figure 5.22. Only the second mode's SLA shows a significant trend.

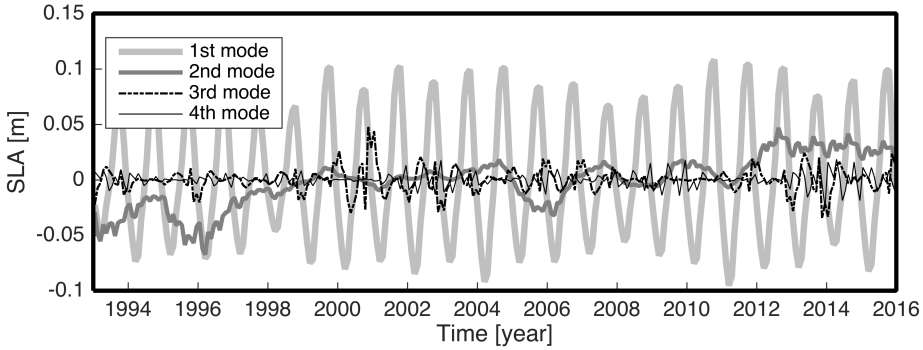

Figure 5.21. Spatial average of decomposed SLA time series from the first to the fourth mode of AVISO-KP

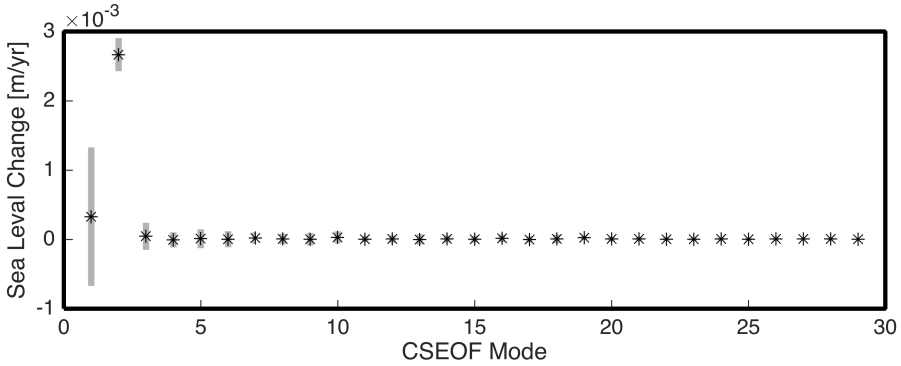

Figure 5.22. Linear trends (black '*') and 95 % confidence intervals (gray line) of the spatially averaged decomposed SLA time series from the first to the fourth mode of AVISO-KP

5.2 Sea Level Reconstruction around the KP

5.2.1 Sea Level Reconstruction applying various data sets

The multivariate regression considering lagged relationship between CSEOF's modes of SST and SLA was applied to reconstruct SLA around the KP over 1900-2014. For these reconstructions, four SST and one wind reanalysis data were used as mentioned in Chapter 4.

Each SST data was divided into three cases: global, NWP, and around the KP. For the wind data, only the NWP region was considered. A total of thirteen cases of reconstructions were conducted and the results are given in Figure **5**.**23** - Figure **5**.**35**.

Most results showed a good agreement with TG MSLA except the case of global HadiSST.

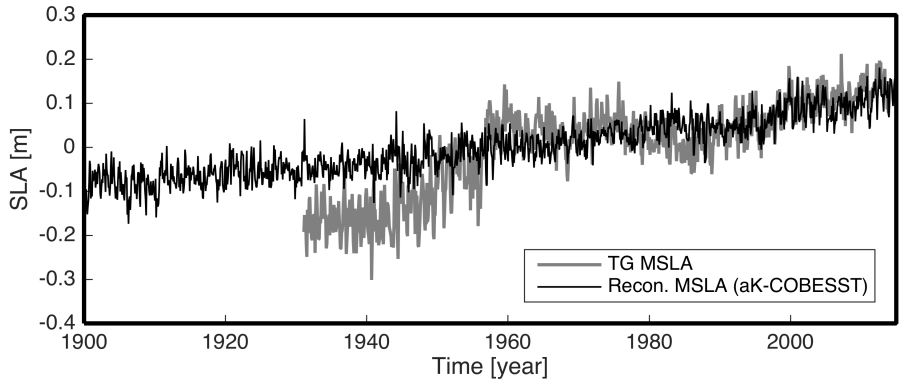

Figure 5.23. Comparison between reconstructed MSLA and the TG MSLA (COBESST around the KP)

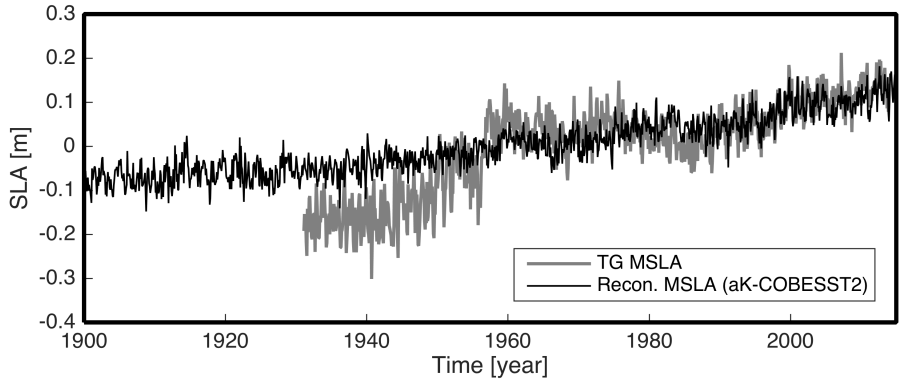

Figure 5.24. Comparison between reconstructed MSLA and the TG MSLA (COBESST2 around the KP)

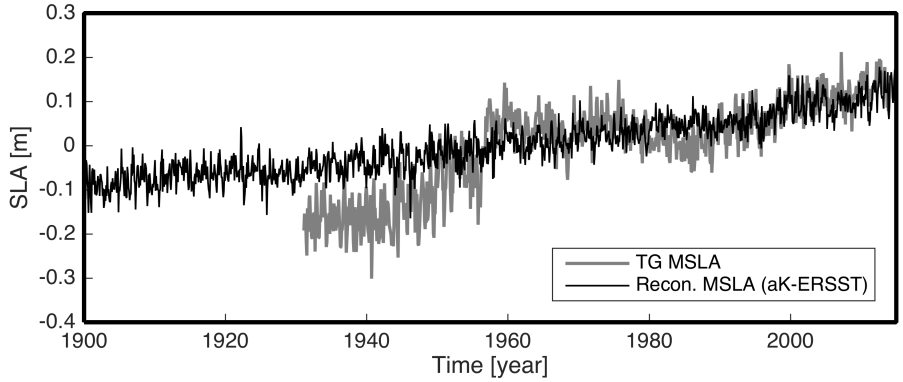

Figure 5.25. Comparison between reconstructed MSLA and the TG MSLA (ERSST around the KP)

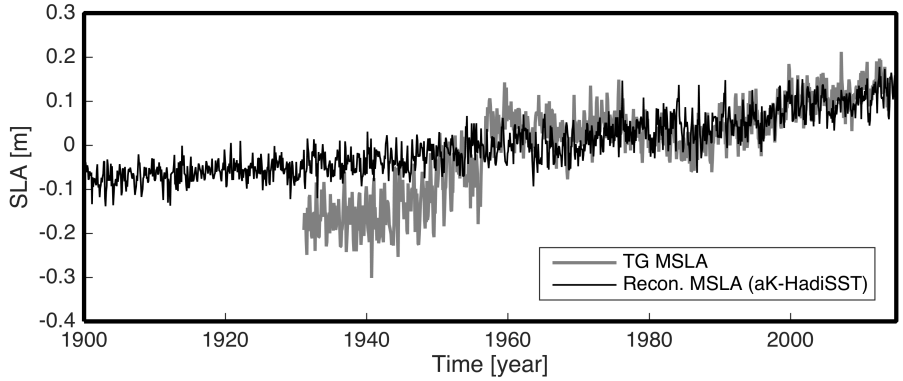

Figure 5.26. Comparison between reconstructed MSLA and the TG MSLA (HadiSST around the KP)

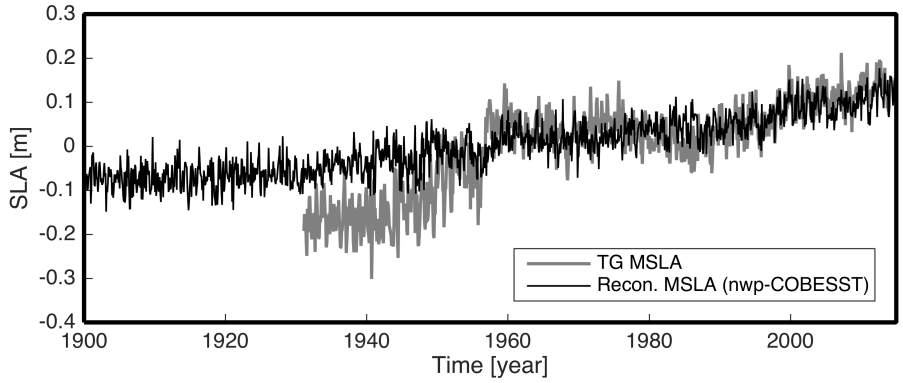

Figure 5.27. Comparison between reconstructed MSLA and the TG MSLA (COBESST of the North-West Pacific)

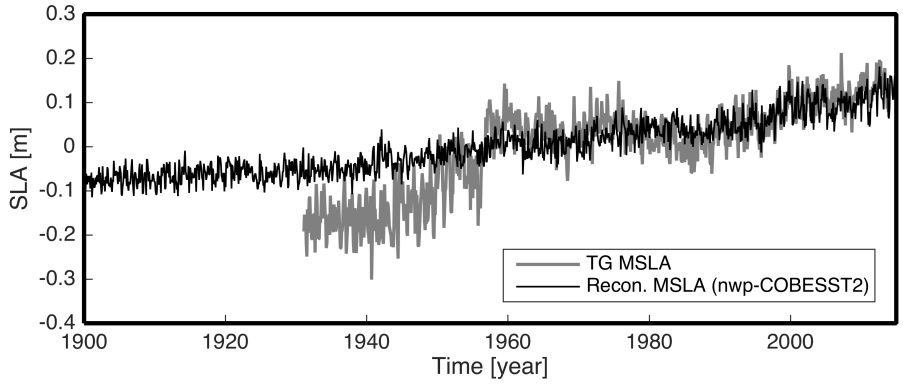

Figure 5.28. Comparison between reconstructed MSLA and the TG MSLA (COBESST2 of the North-West Pacific)

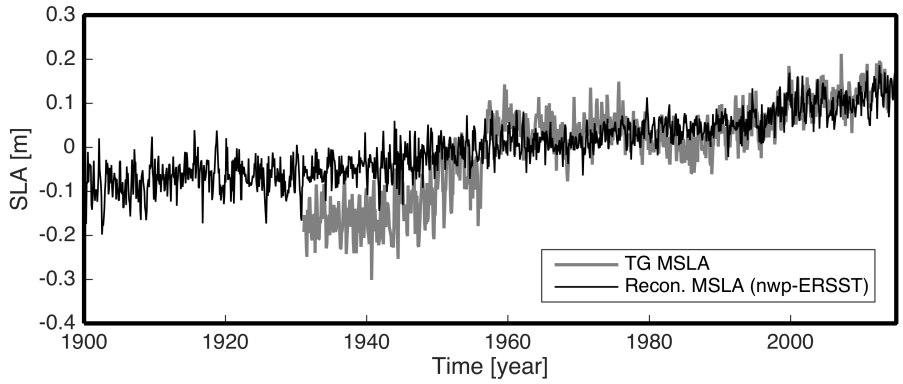

Figure 5.29. Comparison between reconstructed MSLA and the TG MSLA (ERSST of the North-West Pacific)

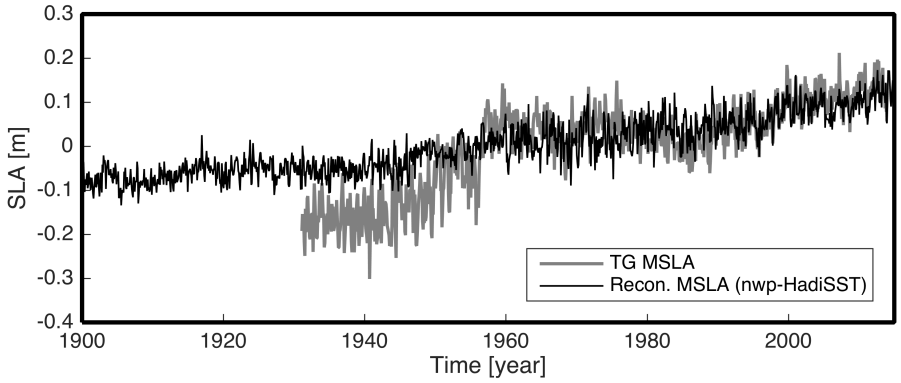

Figure 5.30. Comparison between reconstructed MSLA and the TG MSLA (HadiSST of the North-West Pacific)

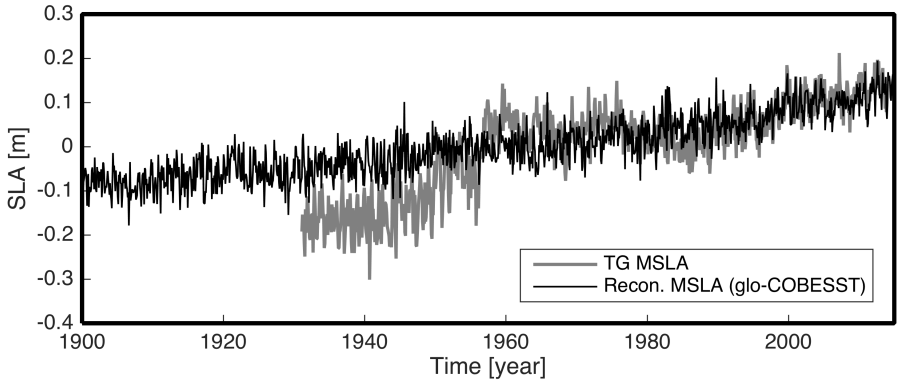

Figure 5.31. Comparison between reconstructed MSLA and the TG MSLA (global COBESST)

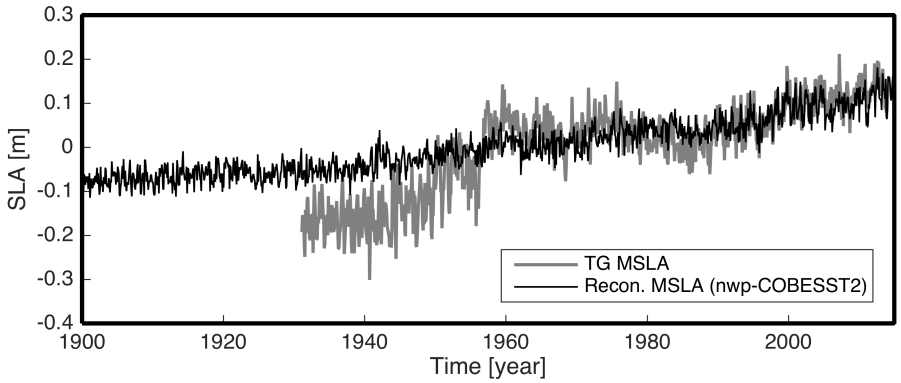

Figure 5.32. Comparison between reconstructed MSLA and the TG MSLA (global COBESST2)

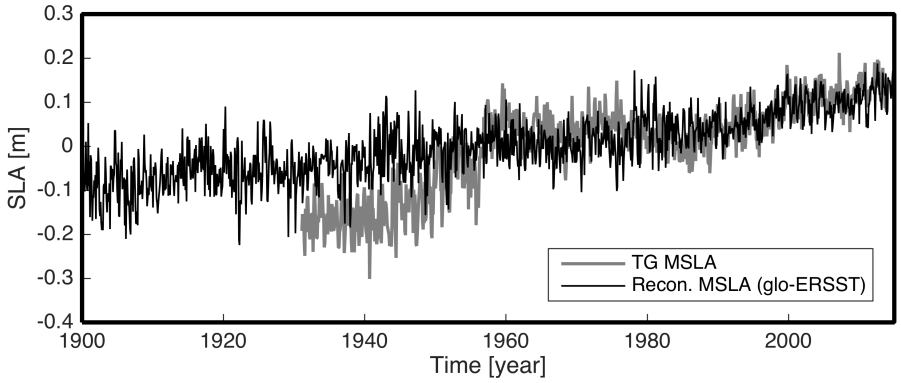

Figure 5.33. Comparison between reconstructed MSLA and the TG MSLA (global ERSST)

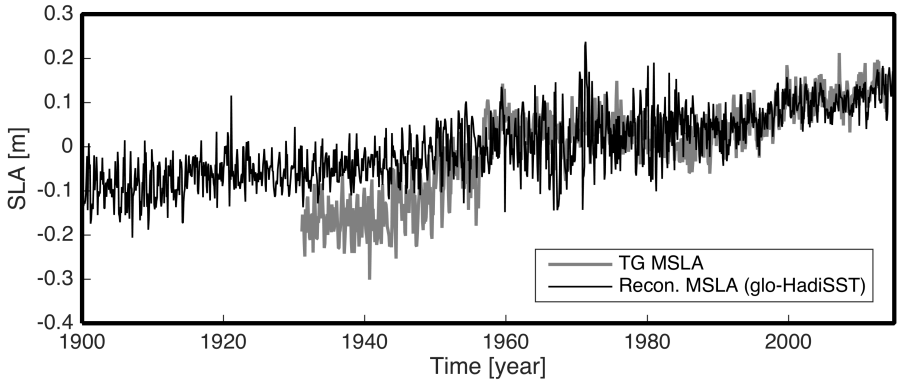

Figure 5.34. Comparison between reconstructed MSLA and the TG MSLA (global HadiSST)

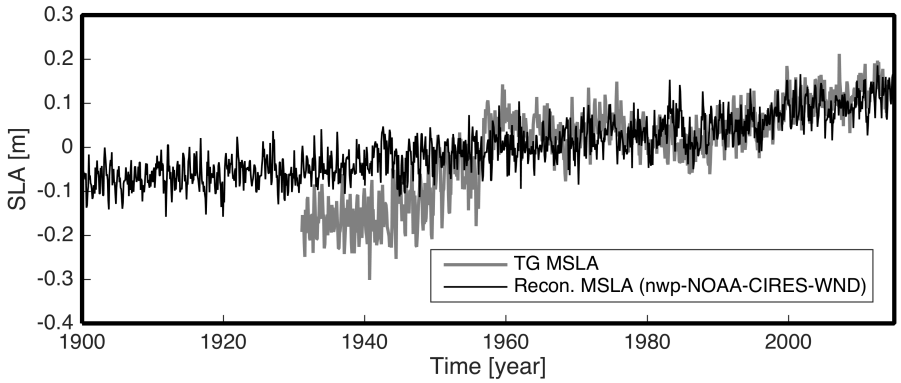

Figure 5.35. Comparison between reconstructed MSLA and the TG MSLA (NOAA-CIRES Wind of the North-West Pacific)

5.2.2 Verification of Sea Level Reconstructions around the KP

The thirteen reconstructions showed a reasonable agreement with TG MSLA over 1965-2014. For the prior period of 1965, however, the results showed considerable diversity. In this section, the reconstructed MSLA-KPs were compared with the previous reconstruction result (Hamlington et al., 2011) and the TG MSLA over 1970-2009 considering the available number of TG data (see Figure 3.2). Both a correlation coefficient and normalized root mean squared error (NRMSE) were applied for the quantified comparison. The comparison result is given in Figure 5.36.

The COBESST2 in NWP Ocean showed the best agreement and both NRMSE and correlation coefficient had better results. On the contrary, the global HadiSST case showed the worst results. The worst and best reconstructions are given in Figure 5.37 - Figure 5.40.

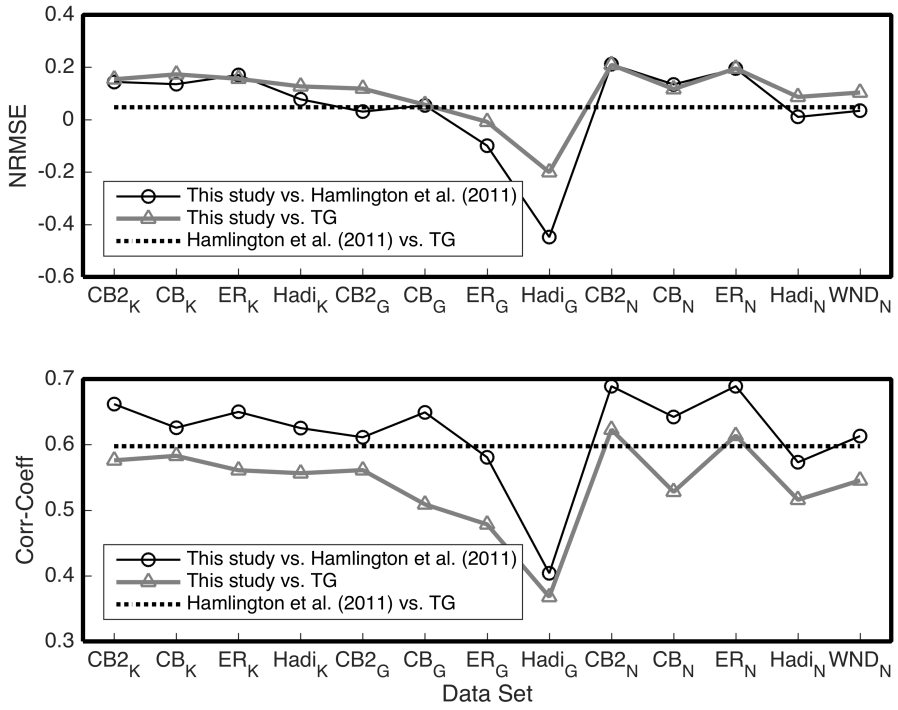

Figure 5.36. Results of goodness of fit test for Reconstructed SLA according to Hamlington et al. (2011) and TG MSLA; the top figure include normalized root mean squared error and the other include the correlation coefficients; here subscripts K, G, and N represent 'around the Korean Peninsula', 'Global', and 'the North-West Pacific', respectively and CB, CB2, ER, Hadi, and WND represent 'COBESST', 'COBESST2', 'ERSST', 'HadiSST', and 'NOAA-CIRES-WND'.

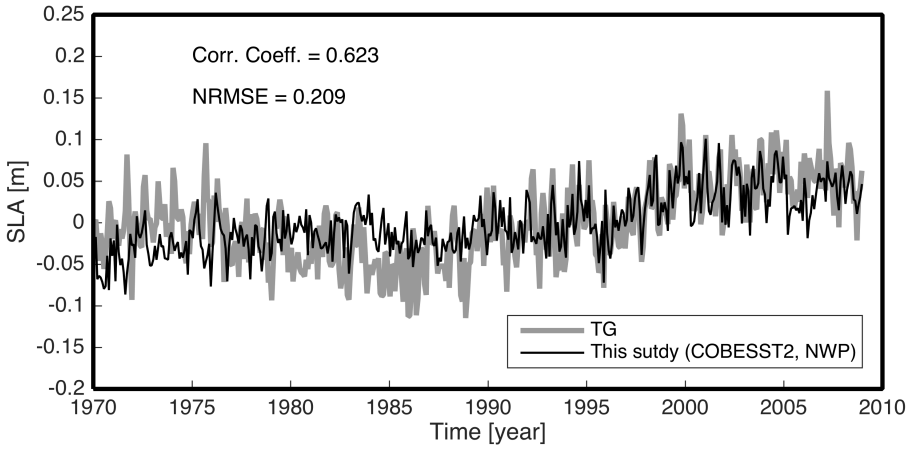

Figure 5.37. The best reconstruction MSLA (COBESST2 of the North-West Pacific Ocean) and Hamlington et al (2011)'s MSLA

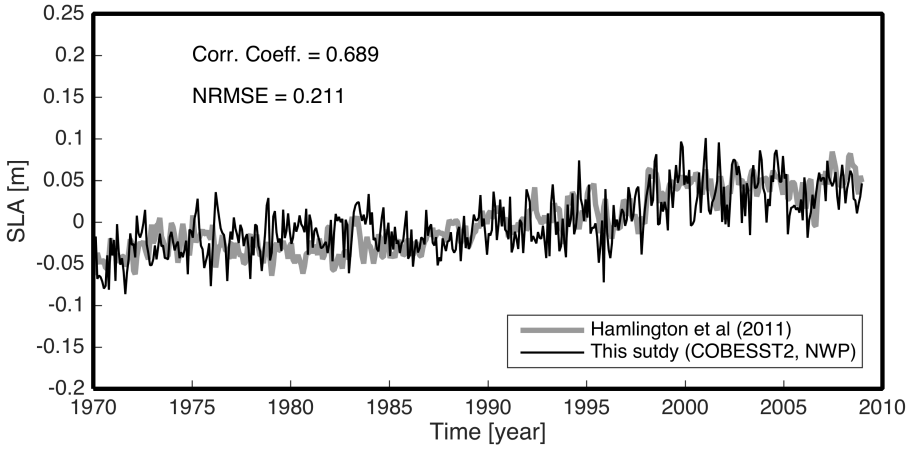

Figure 5.38. The best reconstruction MSLA (COBESST2 of the North-West Pacific Ocean) and TG's MSLA

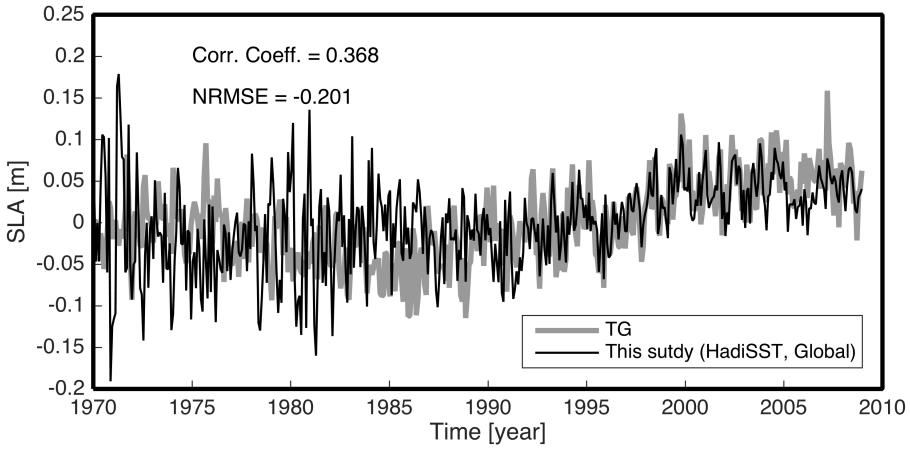

Figure 5.39. The worst reconstruction MSLA (HadiSST in global) and Hamlington et al (2011)'s MSLA

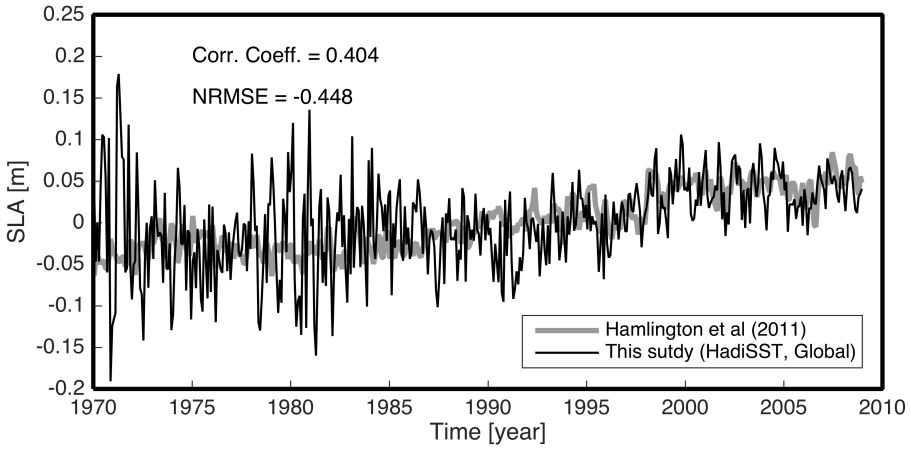

Figure 5.40. The best reconstruction MSLA (HadiSST in global) and TG's MSLA

5.2.3 Estimation of Confidence Interval

Using MC simulation, a 95% confidence interval was estimated based on the best reconstruction case (COBESST2_NWP). Thousand SLA-KPs were generated. By applying the regression coefficients' mean and standard deviation, each mode's PCT was randomly generated, and the process was repeated by thousand times and these PCTs were combined with CSLV's of AVISO-KP.

Through this process, thousand of SLA-KP reconstructions were generated, and the mean and standard deviation were estimated using these. This means that the reconstructed data has their own mean and standard deviation value. An example of reconstruction SLA-KP is given in Figure 5.41 and Figure 5.42. The resulting MSLA-KP and 95% confidence interval are shown in Figure 5.43.

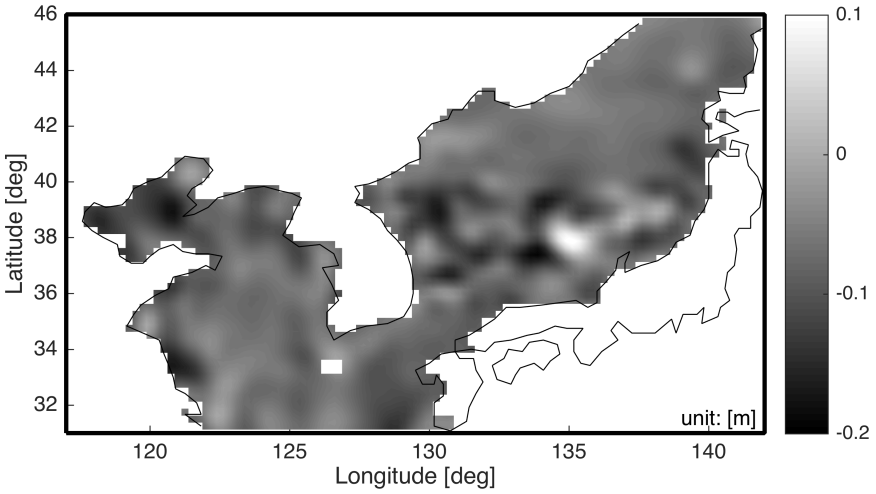

Figure 5.41. Mean value map of reconstructed SLA-KP (Jan. 1970)

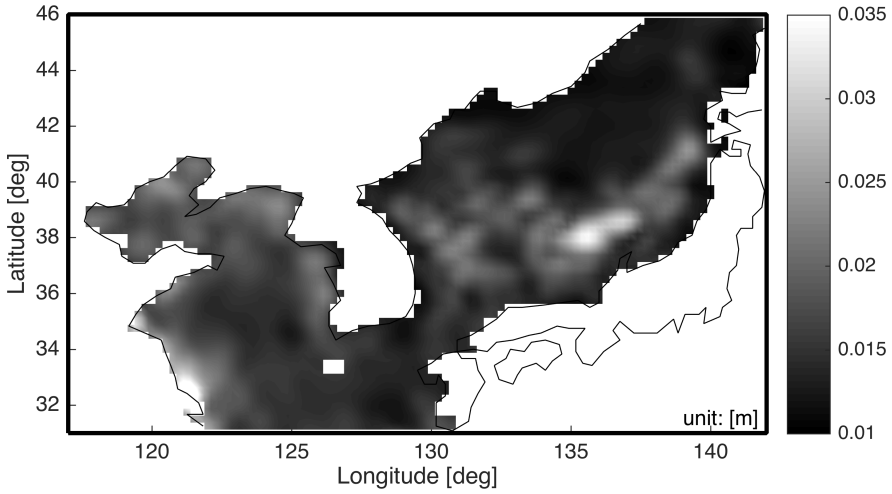

Figure 5.42. Standard deviation value map of reconstructed SLA-KP (Jan. 1970)

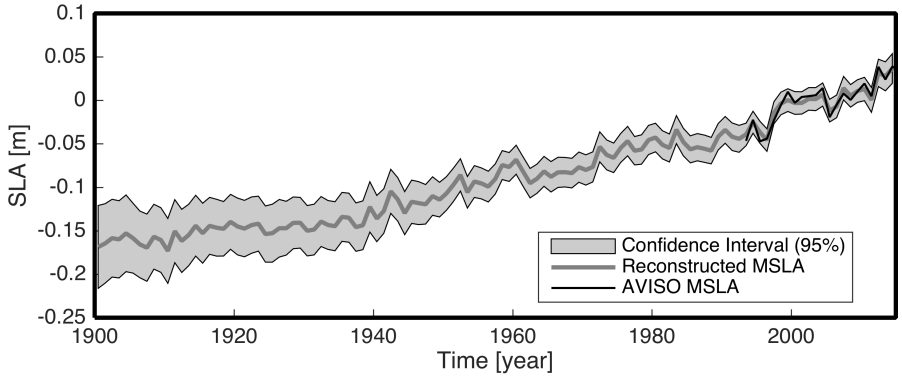

Figure 5.43.The Best reconstructed MSLA (COBESST2 of the North-West Pacific Ocean) and 95% confidence interval.

5.3 Sea Level Projection around the KP

Using the ensemble means of process-based models of CMIP5 (Stocker et al., 2013), the SLA-KPs under RCP scenarios were projected.

The projected SLA-KPs have the similar spatial and periodic variability but the increasing sea level rising trends. The projection results are given in Figure 5.44 - Figure 5.47.

Linear trends for each RCP scenario (RCP 2.6, 4.5, 6.0, and 8.5) were 4.59 mm/yr, 5.46 mm/yr, 5.37 mm/yr and 7.57 mm/yr respectively (see Figure 5.48). Each projection time step has their mean and standard deviation for each spatial grid same as SLA-KP reconstruction result.

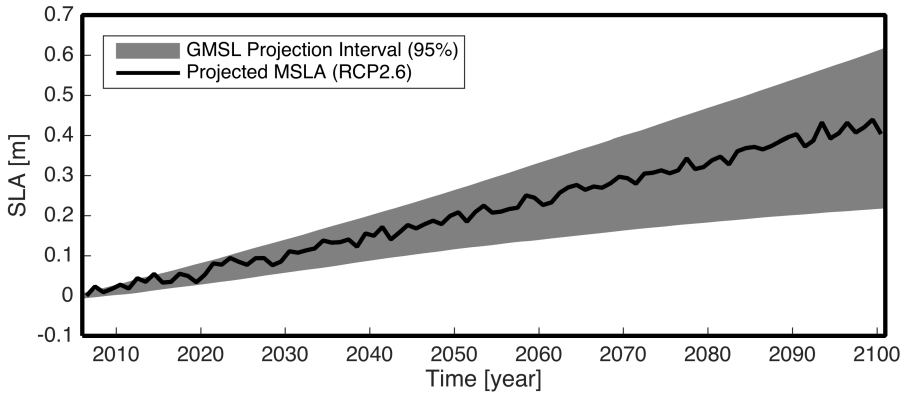

Figure 5.44. Projected MSLA-KP under RCP 2.6 scenario and 95% confidence interval of Global MSLA of RCP 2.6

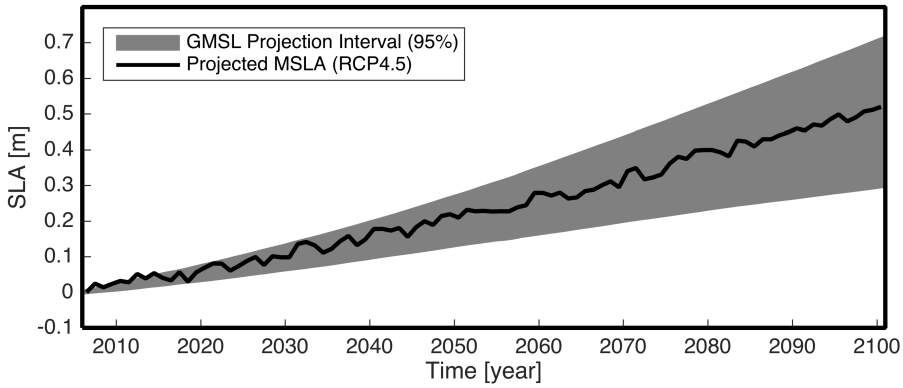

Figure 5.45. Projected MSLA-KP under RCP 4.5 scenario and 95% confidence interval of Global MSLA of RCP 4.5

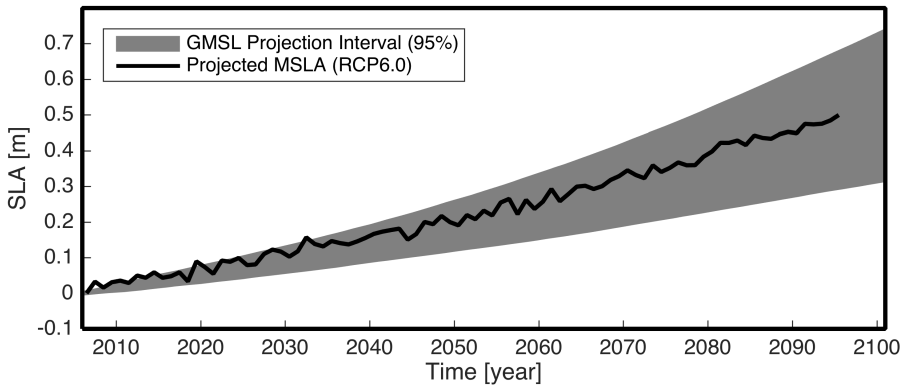

Figure 5.46. Projected MSLA-KP under RCP 6.0 scenario and 95% confidence interval of Global MSLA of RCP 6.0

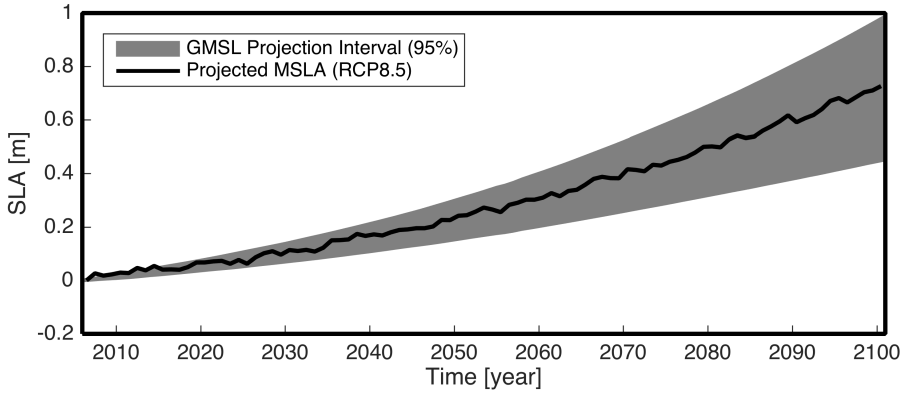

Figure 5.47. Projected MSLA-KP under RCP 8.5 scenario and 95% confidence interval of Global MSLA of RCP 8.5

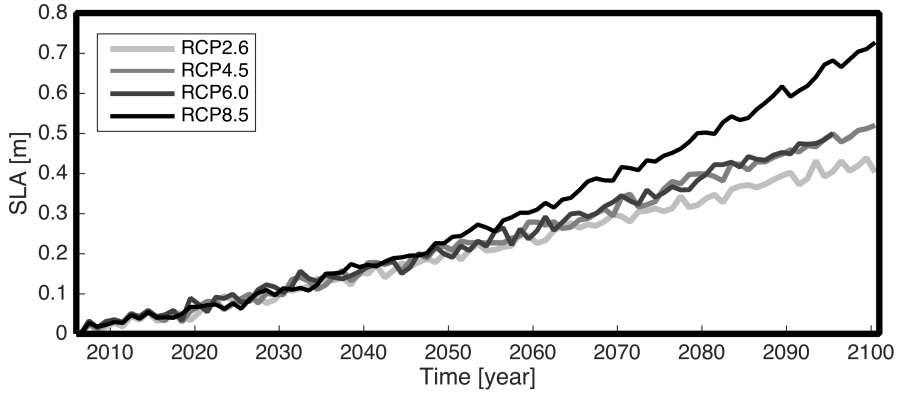

Figure 5.48. Projected MSLA-KP according to RCP scenarios

Chapter 6 Discussion

This Chapter is divided into three sections. The first section presents a brief overview and discussion of the characteristics of sea level anomaly around the Korean Peninsula over the satellite era (1993 - present). The second section includes a discussion of the SLA reconstruction results around the KP over 1900-2014. The last section discusses the SLA projection results over 2006-2099. Each section includes a brief summary and discussion of the section's subject matter.

6.1 Sea Level Anomaly around the KP

The purpose of the study of SLA-KP during the satellite era is to increase our understanding of sea level around the KP before conducting both the reconstruction and projection of SLA-KP. First, to achieve this goal, an agreement between TG-KP and SLA-KP of AVISO was estimated in terms of correlation coefficient (ρ), normalized root mean square error (NRMSE), and linear trend by using averaged time series and individual time series at each TG location. Second, the gravity field variation was investigated to figure out a dominant effect of SLA-KP. Finally the SLA-KP variation caused by the change of continental water mass changes was investigated.

The linear trend of MSLA-KP of AVISO was about 3 mm/yr, similar to the linear trend of global MSLA over 1993-2015, but the spatial pattern of the trend was not simple. Some areas showed trends over 7 mm/yr, while in other regions there were trends less than 1 mm/yr of the linear trend (see Figure **5**.**1**). These uneven patterns originated from two sources; one is river discharge in

the Yellow Sea area, and the other is a vortex induced upwelling and downwelling effect in the East/Japan Sea area. The Dayang, Huli, Yingna, Zhuang, and Xiaosi Rivers flow into the Yellow Sea from China, and Yalu (Amnokgang), Taeryong, Taedong, Han, Geum, Mangyeong, Dongjin, and Yeongsan Rivers discharge into the Yellow Sea. The extreme patterns near the land seem to relate to the variation of river discharge (see Figure **6**.**1**).

In the East/Japan Sea, both warm currents and cold currents exist simultaneously and the borderline repeatedly oscillates up and down. Near the borderline, the warm current and cold current make small gyres, and the gyres make the uneven surface variations. These kinds of relatively large variations make the assessments of the linear trend poor (see Figure **6**.**2**-Figure **6**.**4**).

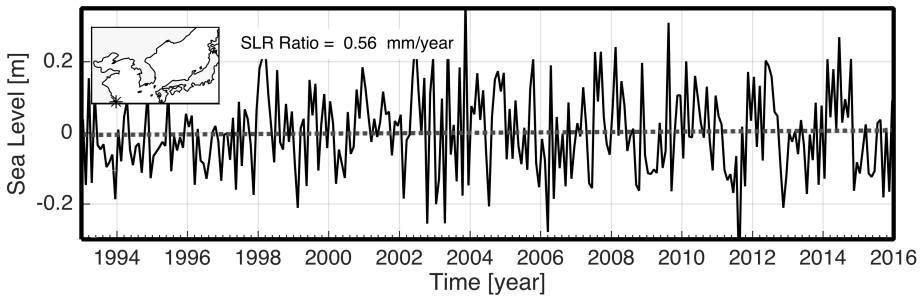

Figure 6.1. SLA time series near the river mouth (Yangtze River)

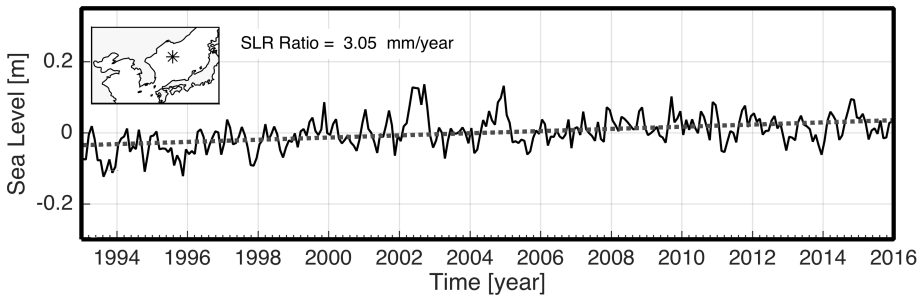

Figure 6.2. SLA time series of less gyre area showing similar linear trend with the MSLA-KP

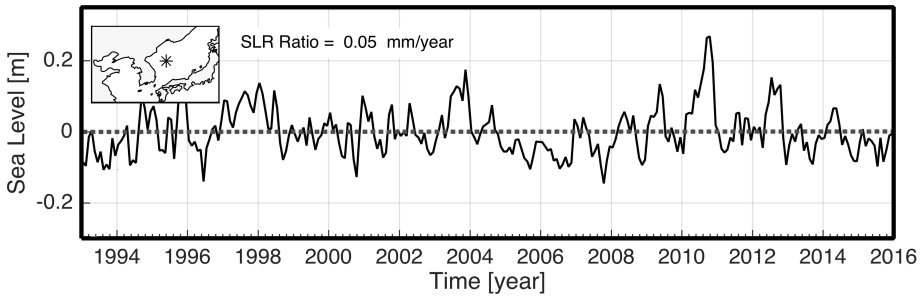

Figure 6.3. SLA time series of gyre area showing lower linear trend comparing with the MSLA-KP

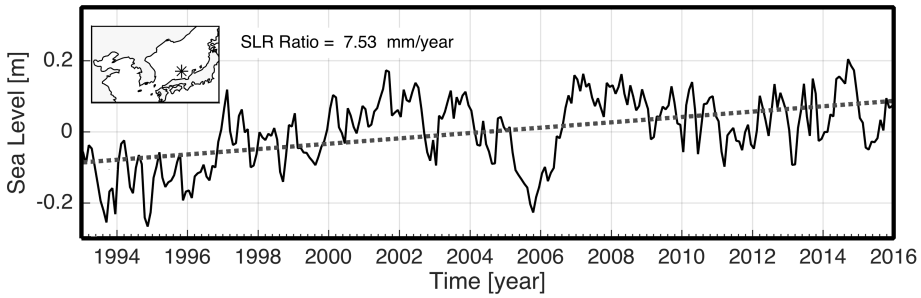

Figure 6.4. SLA time series of gyre area showing higher linear trend comparing with the MSLA-KP

The linear trend at each TG location was estimated and it was compared with the nearest point in AVISO data (see Figure **5**.**3** - Figure **5**.**5**). The comparison showed that only five TGs showed less than 30% of difference with the AVISO's linear trend (see Figure **5**.**5**). Eleven TGs showed less than 30% of underestimation and twenty-one TGs had over than 30% of over estimation.

To figure out the effect of these disagreements, the MSLA-KP of AVISO was compared with the MSLA of TG-KP, and these time series showed $\rho = 0.89$ and NRMSE = 0.52 (see Figure **6**.**5**). The MSLA rise ratio of combined TGs was estimated as 4.31 mm/yr and this value is about 40% higher than the MSLA-KP of AVISO. This disagreement originated from the

short time period and a lack of TGs. With larger numbers of TGs, the errors of each TG data can cancel out.

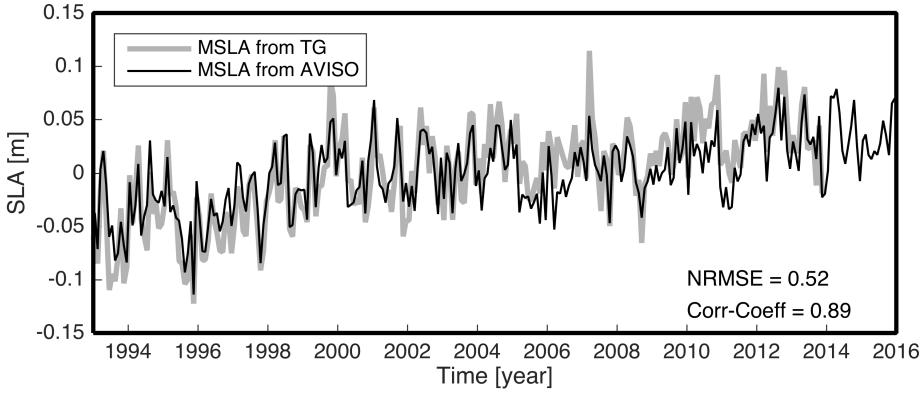

Figure 6.5. MSLA-KP time series of AVISO and TG

Through an investigation of gravity field around the KP, the major driving force of the SLA can be determined. When the gravity field anomaly shows similar variation, the water mass balance is a main factor for the SLA. On the other hand, when the gravity field anomaly shows less variance in comparison to SLA, the thermal expansion is a more important factor for the SLA.

The GRACE-Mascon data was applied for the gravity field investigation, and by comparing the correlation coefficient the dominant effect was estimated. The correlation coefficient in each Mascon was calculated, and using the result the study area was divided into four zones (see Figure **5**.**8**). The Yellow Sea area (Zone I) showed ρ =0.87 and this value is much higher than other areas (Figure **5**.**9** - Figure **5**.**12**). From this, we can say that the dominant effect of SLA for Zone-I is water mass variation. The shallow water depth is not sufficient to show thermal expansion effect (see Figure **6**.**6**). In Zone-II, the correlation coefficient was 0.60, and because the

water depth is deeper than the Zone-I, the effect of thermal expansion is greater than Zone-I. However in Zone-III and IV, the correlation coefficients are 0.10 and -0.11, respectively. In these zones, the water depth is deep enough to show thermal expansion as a dominant factor. An interesting thing is that the gravity fields show negative trends in these two zones after 2011, and it seems to exceed this research's range.

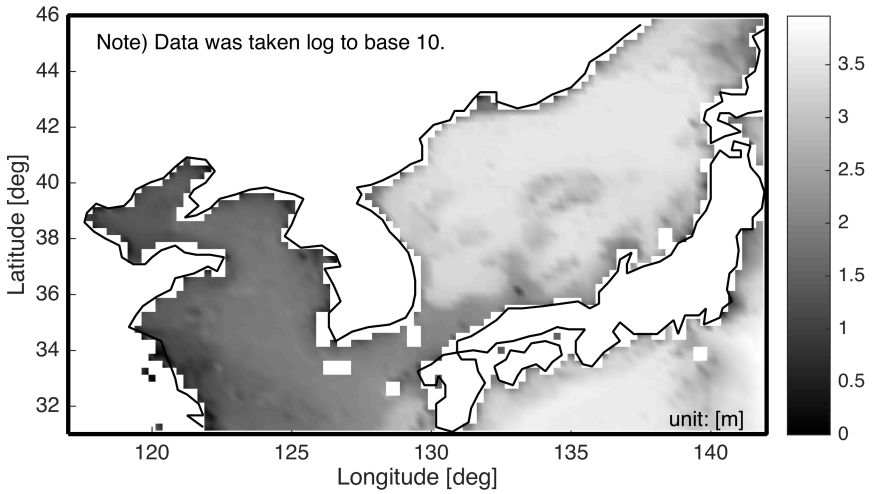

Figure 6.6. Depth map around the KP

Through current analysis, the relationship between mass balance and SLA in each zone was estimated. Three particular transects were investigated, with locations given in Figure 5.13. The velocity balance through the lines was estimated for the near surface area (< 15m). As we can see in Figure 5.13, the velocity balance could not explain the SLA-KP because the variations were biased to positive or negative values, which mean continuous mass loss or accumulation. This analysis, however, can give a clue to understanding what is happening in SLA-KP. The velocity balances have similar patterns in

that they show a high peak in the summer season and low trough in the winter season. The Kuroshio Current is divided into three warm currents - Yellow Sea Warm Current, Tsushima Current, and East Korean Warm Current, and these warm currents are intensified by combining or weakened by separation (Ichikawa and Beardsley, 2002). These kinds of variations force the fluctuations in current velocity through the three lines. The Yellow Sea's shallow water depth also makes this mass balance the dominant effect on SLA. In the East/Japan Sea, however, the velocity balance shows reverse behavior (see Figure 5.14). However, this is opposite from the SLA behavior in the area. From this, it is concluded that the major effect on SLA in Zone-III and IV is the thermal expansions.

The SLA-KP caused by continental water mass balance was estimated by applying the fingerprint map of the previous study (Adhikari and Ivins, 2016). The partial effects on SLA are 0.25 mm/yr, 1.01 mm/yr, 0.41 mm/yr, and 0.01 mm/yr resulting from Antarctic Ice Sheet, Greenland Ice Sheet, Glaciers except for the previous two regions, and the global noncryospheric terrestrial water storage, respectively. The combined SLR ratio is 1.76 mm/yr over 2003-2015 and the SLR ratio map is given Figure **5**.**15**. The effect is getting less toward the western and northern direction, and the maximum difference is about 0.3 mm/yr.

CSEOF decomposition was conducted to investigate periodic orthogonal behaviors for SLA-KP with 12 months nested period after removing mean values at each grid point. The four CSEOF decomposition results are given (see Figure **5**.**16** - Figure 5.22). The first mode represents a seasonal variation considering the CSEOF's SLA patterns and the periodic PCT. Nearly 60% of SLA-KP variations can be presented by this mode. The second mode shows similar spatial patterns having positive value for all

months, and the PCT shows clear increasing trend. This means the second mode is a sea level rising mode, and it represents 10% of variations of SLA-KP roughly. The third and fourth modes were not able to relate to specific phenomenon, and the modes explain SLA-KP at about 5% and 3%, respectively. As can be seen in Figure **5**.**16**, Figure 5.22, and Figure 5.21, using the four modes, we can explain about 75% of SLA-KP. The first and second modes have the linear trend, but the linear trend in the first mode is negligibly small comparing the signal itself. Hence we can say that the second mode is the most important key to estimating the sea level rise around the KP.

6.2 Sea Level Reconstruction around the KP

Thirteen SLA-KPs were reconstructed over 1900-2014 by using the combination of different data sets and domains. To select the best reconstruction, MSLA of TG over 1970-2013 and MSLA of Hamlington et al. (2011) over 1970-2008 were used as the reference data, and the reconstructed MSLAs were compared with these two references. The comparison time period started from 1970, because the number of TGs that had a great effect on a quality of reconstruction was less than 20. For the quantified comparison, correlation coefficient (ρ) and NRMSE values were used.

The best reconstruction among the 13 reconstructed SLA-KPs is the case that used North-West Pacific area of COBESST2. The reconstruction showed better agreement than the reconstruction of Hamlington et al. (2011) without using TG data during the reconstruction process.

The reconstructed MSLA-KP shows good agreement with other reference MSLA-KPs but TG data. But the disagreement is caused by lack of TGs before 1970. The reconstruction of this study shows better agreement with the AVISO's MSLA-KP, also has more fluctuations which are important to apply this results for engineering purposes. These detailed fluctuations are closer to the real signals. This is related to the applied number of modes for the reconstruction process. Hamlington et al. (2011) used a limited number of CSEOF modes to avoid over-fitting issues, but in the study, nineteen CSEOF modes are used which explain 98% of total variance of SLA-KP.

The linear trend in SLA-KP over 1900-2014 is estimated as 1.71 ± 0.04 mm/yr, and this value is similar to the linear trend of Church and White (2011) as 1.70 ± 0.02 mm/yr. A linear trend at each grid point of AVISO sea level anomaly data was calculated (Figure **6**.**8**), and the maximum and minimum

linear trends are about 2.1 mm/yr and 1.4 mm/yr, respectively. The variation of the linear trends on the trend map of this study is much less than the satellite data. This means that the long time period reduced the effect of large amplitude signals. Especially, the high trends in the areas where high trends were shown in the Yellow Sea were weakened significantly (Figure **5**.**1**).

Each zone's MSLA was estimated and the result is given in Figure **6**.**9**. As can be seen in the figure, the Zone-I and III shows larger variations. The shallow water depth and sea surface lifting effect of Ekman transport is meant to be the main reasons for these larger variations for each zone.

By conducting a thousand reconstructions considering the standard deviations of each PCT's regression coefficient and GMSL, the confidence intervals of reconstructed SLA-KP were calculated over the entire period. Each grid has mean and standard deviation for each time step.

KHOA (Korea Hydrographic and Oceanographic Agency) has provided a SLR report around the KP using TG data and the report has been updated annually. To give a comparison between the KHOA's SLR and this study's result, the SLR of current research in the same location of TGs that is used for the SLR report (see Figure **6**.**10**).

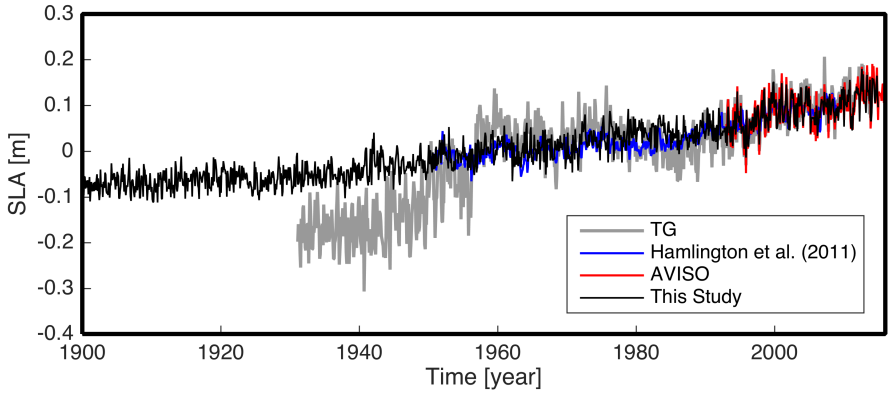

Figure 6.7. Comparison between the reconstructed MSLA-KP and other reference MSLA-KPs

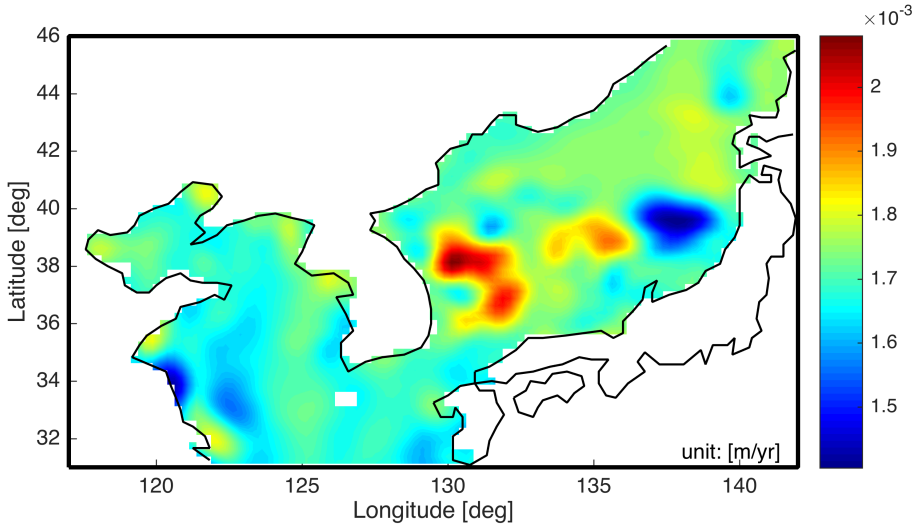

Figure 6.8. Linear trend map of the reconstructed SLA-KP over 1900-2014

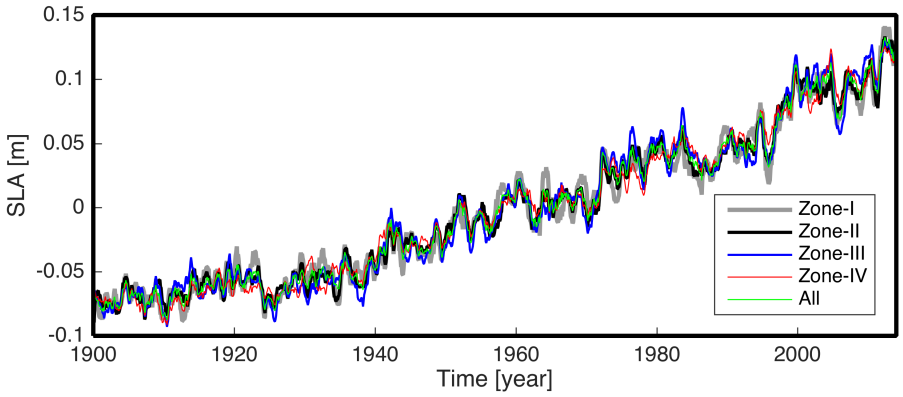

Figure 6.9. MSLA for each zone.

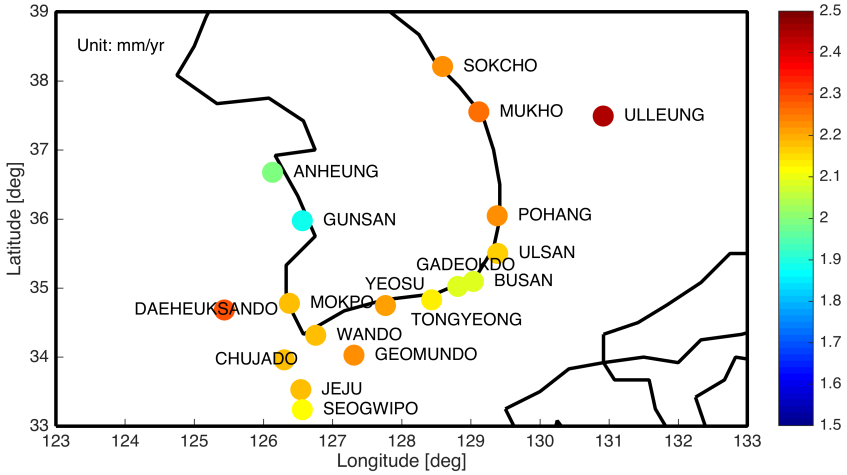

Figure 6.10. Sea level rise ratio at TG stations around the KP over 1960-present

6.3 Sea Level Projection around the KP

The process of the projection of SLA-KP is similar to the reconstruction process in all aspects except using simulated SSTs and simulated GMSL with RCP scenarios. The PCTs of each mode of CSEOF LVs were extended into future using the simulated SSTs of AOGCM model with RCP scenarios. After projecting the future SLA-KPs without GMSL, the ensemble means of RCP scenarios were added to them.

The SLR ratios over 2006 to 2100 were estimated as follows with 95% of confidence interval: 4.59 ± 2.01 mm/yr (RCP 2.6), 5.46 ± 2.17 mm/yr (RCP 4.5), 5.37 ± 2.13 mm/yr (RCP 6.0), and 7.57 ± 2.69 mm/yr (RCP 8.5). Applying the estimated SLR ratios, the sea level is projected to be increased in 2100 as follows: 43.2 ± 18.3 cm (RCP 2.6), 51.3 ± 19.3 cm (RCP 4.5), 50.5 ± 19.0 cm (RCP 6.0), and 71.2 ± 23.1 cm (RCP 8.5).

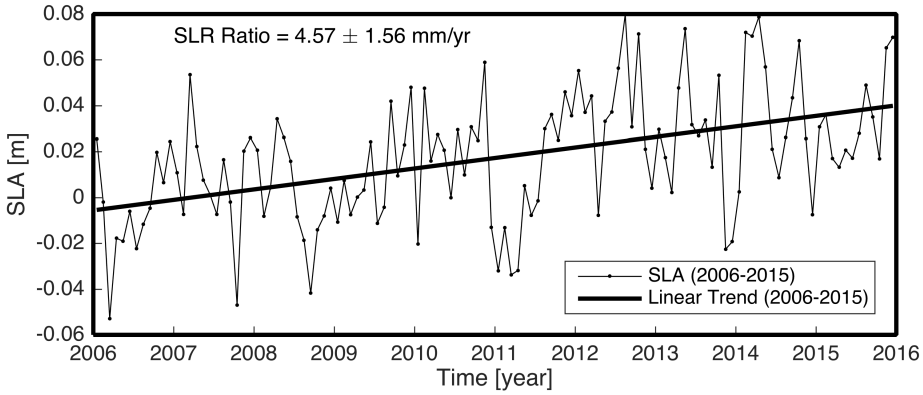

Figure 6.11. MSLA and the linear trend line over 2006-2015

Using the AVISO data, the actual sea level rise ratio around the KP from 2006 to 2015 is estimated as 4.57 ± 1.56 mm/yr, and this value is very similar to the RCP 2.6's sea level rise ratio (see Figure **6**.**11**). It seems to be a

reasonable result, but the current sea level change most likely is related to the PDO (Hamlington et al., 2016). Therefore a longer observation is necessary to realize the current situation.

The sea level rising scenarios from GCM models do not represent the specific characteristics of SLA-KP such as sea level lifting by vortex and significant variation near the river mouths (see Figure 6.12 and Figure 6.13). The most important meaning of this projection is providing the sea level rising scenarios that have the similar characteristics with the real SLA-KP having high resolution.

Same as the reconstructed SLA-KP, the projected SLA-KP provides the mean and standard deviation at each grid point and time step. Using this data engineers can generate random SLA-KPs for answering their purpose.

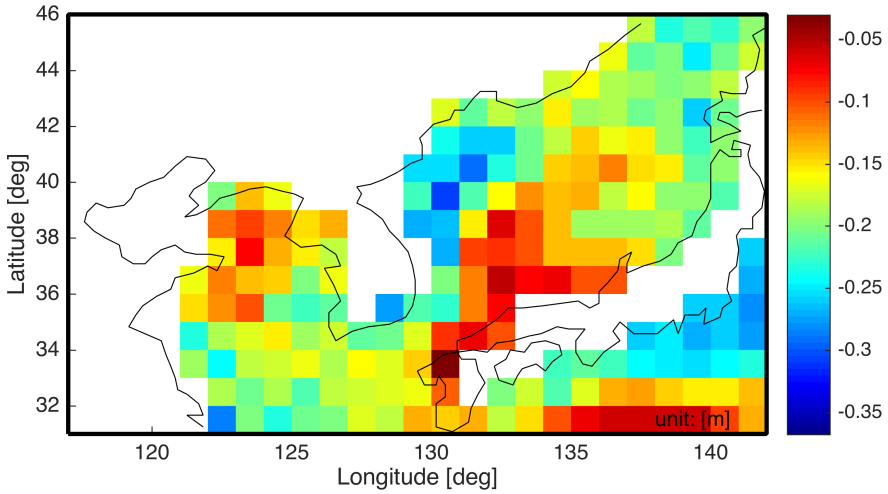

Figure 6.12. SLA-KP of HadGEM2-ES (RCP 2.6; r2i1p1; Sep., 2006)

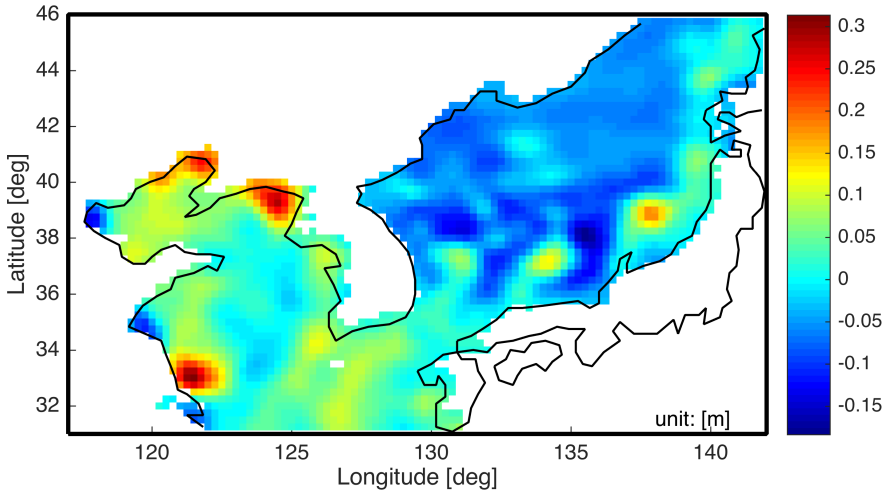

Figure 6.13. SLA-KP of AVISO (Sep., 2006)

Chapter 7 Conclusion

The primary purposes of this research are as in the following: 1) What are main characteristics of SLA-KP. 2) How can we reconstruct the past SLA-KP where the TG observations were not enough? 3) What is the sea level anomaly around the Korean Peninsula over 1900-2014? 4) How can we project the future SLA-KP through the RCP scenarios? 5) What is the sea level anomaly around the Korean Peninsula over 2006-2100?

To investigate the characteristics of SLA-KP, the following data were used: the data of satellite altimeter (AVISO), satellite gravity field measurement (GRACE-Mascon), sea level fingerprints associating ice thickness in glaciers and global noncryospheric terrestrial water storage, and TG from PSMSL. By comparing the SLA between GRACE-Mascon and AVISO, we concluded that the main driving force of SLA in the Yellow Sea was a mass balance; on the other hand, the thermal expansion was the dominant cause of SLA in East/Japan Sea. The sea level rise trend over the domain was estimated as 3.1 ± 0.5 mm/yr; however, when we look into the trend map, some areas (such as near the river mouth in the Yellow Sea and in the middle of the East/Japan Sea) had abnormal values. These unusual values were originated by the irregular river discharges and sea level lifting effect by the vortex. From the sea level fingerprints, the SLR around the KP from the ice melting and the change of the continental water storage except the glacier amount was estimated as 1.76 mm/yr. The SLA-KP has seasonal variations; the sea level is dropping during the winter period and is rising for the summer

season and these seasonal alterations are starting from the Yellow Sea and spread out the East/Japan Sea.

The reconstruction was performed using SLA-KP of AVISO-KP, SST data from four different reanalysis data sets, and wind reanalysis data. Each SST data was divided into three cases (global, North-west Pacific, around the Korean Peninsula) and the wind reanalysis data was trimmed around the North-west Pacific area. The thirteen data sets were decomposed by CSEOF decomposition; the AVISO-KP was disintegrated into CSEOF modes after removing the GMSL. The decomposed CSEOF modes' CSLV played a role of basis functions for the reconstruction, and the main process of reconstruction was extending the PCTs of each mode into the past. Each PCT of the AVISO-KP was regressed by the SST's PCTs over the satellite era, and the finding relations were used to extend the AVISO-KP's PCTs. And the extended PCTs were combined to the CSLVs to achieve the reconstructed SLA-KP without global mean SLA. Finally, the GMSL was added to the reconstructed SLA-KP. The thirteen reconstructed SLA-KPs were generated by this study. Using the correlation coefficient and the normal root mean squared error, the best reconstruction was selected; the best reconstruction was produced by COBESST2 data of the North-west Pacific area; through the best reconstruction results, the linear trend of SLA-KP was estimated as 1.71 ± 0.04 mm/yr. The most extreme linear trends didn't appear in the reconstructed SLA-KP. This reconstruction showed better agreement than the previous study's result. Hence we can say that the current reconstruction scheme can be a good alternative for the regions having a few TG data.

The SLA-KP projections were performed corresponding to RCP scenarios (RCP 2.6, 4.5, 6.0 and 8.5) over 2006-2100. The projection process was similar to the reconstruction scheme in the view of using CSEOF's

CSLVs of AVISO data as basis functions. However, the extension data was different. Using CSEOF regression coefficients extended each decomposed PCT. The remaining processes were same with the reconstruction scheme except combining the ensemble means of each scenario's GMSL instead of observed GMSL. The projected SLR ratios over 2006-2100 were estimated as follows with 95% of confidence interval: 4.59 ± 2.01 mm/yr (RCP 2.6), 5.46 ± 2.17 mm/yr (RCP 4.5), 5.37 ± 2.13 mm/yr (RCP 6.0), and 7.57 ± 2.69 mm/yr (RCP 8.5). Applying the estimated SLR ratios, the sea level is projected to be increased in 2100 as follows: 43.2 ± 18.3 cm (RCP 2.6), 51.3 ± 19.3 cm (RCP 4.5), 50.5 ± 19.0 cm (RCP 6.0), and 71.2 ± 23.1 cm (RCP 8.5).

Each projected SLA-KP provides us with the mean and standard deviation for each time step and grid. Through this projection, we can produce SLA-KPs under four RCP scenarios over 2006-2100; and the projected SLA-KP not only preserved the characteristics of the domain but had high resolution same as the AVISO-KP.

Further research is recommended for different areas such as the Indian Ocean and the Antarctic Ocean where it has only a few TGs over the domain. The current reconstructions over these domains do not show good agreement with observations, and the spatial patterns of SLA are much complicated than the SLA-KP, and which makes the reconstruction using the TGs to have poor results. The proposed scheme that has no use of TGs can be a good alternative for the previous reconstruction schemes.

References

Adhikari, S., and Ivins, E. R. (2016). Climate-driven polar motion: 2003–2015. *Science advances* **2**, e1501693.

Barnier, B., Brodeau, L., Le Sommer, J., Molines, J.-M., Penduff, T., Theetten, S., Treguier, A.-M., Madec, G., Biastoch, A., and Böning, C. W. (2007). Eddy-permitting ocean circulation hindcasts of past decades. *Clivar Exchanges* **42**, 8-10.

Bergé-Nguyen, M., Cazenave, A., Lombard, A., Llovel, W., Viarre, J., and Cretaux, J.-F. (2008). Reconstruction of past decades sea level using thermosteric sea level, tide gauge, satellite altimetry and ocean reanalysis data. *Global and Planetary Change* **62**, 1-13.

Bilbao, R. A., Gregory, J. M., and Bouttes, N. (2015). Analysis of the regional pattern of sea level change due to ocean dynamics and density change for 1993–2099 in observations and CMIP5 AOGCMs. *Climate Dynamics* **45**, 2647-2666.

Bojariu, R., and Gimeno, L. (2003). The role of snow cover fluctuations in multiannual NAO persistence. *Geophysical Research Letters* **30**.

Bouttes, N., and Gregory, J. (2014). Attribution of the spatial pattern of CO2-forced sea level change to ocean surface flux changes. *Environmental Research Letters* **9**, 034004.

Box, G. E., Jenkins, G. M., Reinsel, G. C., and Ljung, G. M. (2015). "Time series analysis: forecasting and control," John Wiley & Sons.

Calafat, F. M., and Gomis, D. (2009). Reconstruction of Mediterranean sea level fields for the period 1945–2000. *Global and Planetary Change* **66**, 225-234.

Calafat, F. M., Gomis, D., and Marcos, M. (2009). Comparison of Mediterranean sea level fields for the period 1961–2000 as given by a data reconstruction and a 3D model. *Global and Planetary Change* **68**, 175-184.

Calafat, F. M., and Jordà, G. (2011). A Mediterranean sea level reconstruction (1950–2008) with error budget estimates. *Global and Planetary Change* **79**, 118-133.

Carton, J. A., and Giese, B. S. (2008). A reanalysis of ocean climate using Simple Ocean Data Assimilation (SODA). *Monthly Weather Review* **136**, 2999-3017.

Carton, J. A., Giese, B. S., and Grodsky, S. A. (2005). Sea level rise and the warming of the oceans in the Simple Ocean Data Assimilation (SODA) ocean reanalysis. *Journal of Geophysical Research: Oceans* **110**.

Chambers, D. P., Mehlhaff, C. A., Urban, T. J., Fujii, D., and Nerem, R. S. (2002). Low-frequency variations in global mean sea level: 1950–2000. *Journal of Geophysical Research: Oceans* **107**.

Choblet, G., Husson, L., and Bodin, T. (2014). Probabilistic surface reconstruction of coastal sea level rise during the twentieth century. *Journal of Geophysical Research: Solid Earth* **119**, 9206-9236.

Church, J. A., Clark, P. U., Cazenave, A., Gregory, J. M., Jevrejeva, S., Levermann, A., Merrifield, M. A., Milne, G. A., Nerem, R. S., and Nunn, P. D. (2013). "Sea level change." PM Cambridge University Press.

Church, J. A., and White, N. J. (2006). A 20th century acceleration in global sea-level rise. *Geophysical research letters* **33**.

Church, J. A., and White, N. J. (2011). Sea-level rise from the late 19th to the early 21st century. *Surveys in Geophysics* **32**, 585-602.

Church, J. A., White, N. J., Coleman, R., Lambeck, K., and Mitrovica, J. X. (2004). Estimates of the regional distribution of sea level rise over the 1950-2000 period. *Journal of Climate* **17**, 2609-2625.

Collins, W., Bellouin, N., Doutriaux-Boucher, M., Gedney, N., Hinton, T., Jones, C., Liddicoat, S., Martin, G., O'Connor, F., and Rae, J. (2008). Evaluation of the HadGEM2 model. *Hadley Cent. Tech. Note* **74**.

Compo, G. P., Whitaker, J. S., and Sardeshmukh, P. D. (2006). Feasibility of a 100-year reanalysis using only surface pressure data. *Bulletin of the American Meteorological Society* **87**, 175.

Compo, G. P., Whitaker, J. S., Sardeshmukh, P. D., Matsui, N., Allan, R. J., Yin, X., Gleason, B. E., Vose, R., Rutledge, G., and Bessemoulin, P. (2011). The twentieth century reanalysis project. *Quarterly Journal of the Royal Meteorological Society* **137**, 1-28.

de Vries, H., Katsman, C., and Drijfhout, S. (2014). Constructing scenarios of regional sea level change using global temperature pathways. *Environmental Research Letters* **9**, 115007.

Delecluse, P., Imbard, M., and Levy, C. (1998). OPA 8.1 ocean general circulation model reference manual. *Notes du Pole de Modelisation de l'Institut Pierre-Simon Laplace* **11**, 91.

Dettinger, M. D., Cayan, D. R., Diaz, H. F., and Meko, D. M. (1998). North-south precipitation patterns in western North America on interannual-to-decadal timescales. *Journal of Climate* **11**, 3095-3111.

Farrell, W., and Clark, J. A. (1976). On postglacial sea level. *Geophysical Journal International* **46**, 647-667.

Folland, C., and Parker, D. (1995). Correction of instrumental biases in historical sea surface temperature data. *Quarterly Journal of the Royal Meteorological Society* **121**, 319-367.

Geruo, A., Wahr, J., and Zhong, S. (2013). Computations of the viscoelastic response of a 3-D compressible Earth to surface loading: an application to Glacial Isostatic Adjustment in Antarctica and Canada. *Geophysical Journal International* **192**, 557-572.

Hamlet, A. F., Mote, P. W., Clark, M. P., and Lettenmaier, D. P. (2005). Effects of temperature and precipitation variability on snowpack trends in the Western United States*. *Journal of Climate* **18**, 4545-4561.

Hamlington, B., Cheon, S., Thompson, P., Merrifield, M., Nerem, R., Leben, R., and Kim, K. Y. (2016). An ongoing shift in Pacific Ocean sea level. *Journal of Geophysical Research: Oceans*.

Hamlington, B., Leben, R., and Kim, K. Y. (2012a). Improving sea level reconstructions using non-sea level measurements. *Journal of Geophysical Research: Oceans* **117**.

Hamlington, B., Leben, R., Nerem, R., Han, W., and Kim, K. Y. (2011). Reconstructing sea level using cyclostationary empirical orthogonal functions. *Journal of Geophysical Research: Oceans* **116**.

Hamlington, B., Leben, R., Wright, L., and Kim, K.-Y. (2012b). Regional sea level reconstruction in the Pacific ocean. *Marine Geodesy* **35**, 98-117.

Han, G., Ma, Z., Bao, H., and Slangen, A. (2014). Regional differences of relative sea level changes in the Northwest Atlantic: Historical trends and future projections. *Journal of Geophysical Research: Oceans* **119**, 156-164.

Han, G., Ma, Z., Chen, N., Thomson, R., and Slangen, A. (2015). Changes in mean relative sea level around Canada in the twentieth and twenty-first centuries. *Atmosphere-Ocean* **53**, 452-463.

Hay, C. C., Morrow, E., Kopp, R. E., and Mitrovica, J. X. (2013). Estimating the sources of global sea level rise with data assimilation techniques. *Proceedings of the National Academy of Sciences* **110**, 3692-3699.

Hay, C. C., Morrow, E., Kopp, R. E., and Mitrovica, J. X. (2015). Probabilistic reanalysis of twentieth-century sea-level rise. *Nature* **517**, 481-484.

Hendon, H. H., Wheeler, M. C., and Zhang, C. (2007). Seasonal dependence of the MJO-ENSO relationship. *Journal of Climate* **20**, 531-543.

Hirahara, S., Ishii, M., and Fukuda, Y. (2014). Centennial-scale sea surface temperature analysis and its uncertainty. *Journal of Climate* **27**, 57-75.

Hoffman, J. S. (1984). Estimates of future sea level rise. *Greenhouse effect and sea level rise*, 79-103.

Hoffman, J. S., Keyes, D. L., and Titus, J. G. (1983). "Projecting future sea level rise: methodology, estimates to the year 2100, and research needs," Strategic Studies Staff, Office of Policy Analysis, Office of Policy and Resource Management, US Environmental Protection Agency.

Huang, B., Banzon, V. F., Freeman, E., Lawrimore, J., Liu, W., Peterson, T. C., Smith, T. M., Thorne, P. W., Woodruff, S. D., and Zhang, H.-M. (2015a). Extended reconstructed sea surface temperature version 4 (ERSST. v4). Part I: upgrades and intercomparisons. *Journal of Climate* **28**, 911-930.

Huang, B., Thorne, P. W., Smith, T. M., Liu, W., Lawrimore, J., Banzon, V. F., Zhang, H.-M., Peterson, T. C., and Menne, M. (2015b). Further Exploring and Quantifying Uncertainties for Extended Reconstructed Sea Surface Temperature (ERSST) Version 4 (v4). *Journal of Climate*.

Ichikawa, H., and Beardsley, R. C. (2002). The current system in the Yellow and East China Seas. *Journal of Oceanography* **58**, 77-92.

Ishii, M., Shouji, A., Sugimoto, S., and Matsumoto, T. (2005). Objective analyses of sea-surface temperature and marine meteorological variables for the 20th century using ICOADS and the Kobe collection. *International Journal of Climatology* **25**, 865-879.

Kaplan, A., Cane, M. A., Kushnir, Y., Clement, A. C., Blumenthal, M. B., and Rajagopalan, B. (1998). Analyses of global sea surface temperature 1856–1991. *Journal of Geophysical Research: Oceans* **103**, 18567-18589.

Kaplan, A., Kushnir, Y., and Cane, M. A. (2000). Reduced space optimal interpolation of historical marine sea level pressure: 1854-1992*. *Journal of Climate* **13**, 2987-3002.

Kawamura, R., Suppiah, R., Collier, M. A., and Gordon, H. B. (2004). Lagged relationships between ENSO and the Asian Summer Monsoon in the CSIRO coupled model. *Geophysical Research Letters* **31**.

Kim, K.-Y., and Chung, C. (2001). On the evolution of the annual cycle in the tropical Pacific. *Journal of climate* **14**, 991-994.

Kim, K.-Y., Hamlington, B., and Na, H. (2015). Theoretical foundation of cyclostationary EOF analysis for geophysical and climatic variables: concepts and examples. *Earth-Science Reviews* **150**, 201-218.

Kim, K.-Y., and North, G. R. (1997). EOFs of harmonizable cyclostationary processes. *Journal of the atmospheric sciences* **54**, 2416-2427.

Kim, K.-Y., North, G. R., and Huang, J. (1996). EOFs of one-dimensional cyclostationary time series: Computations, examples, and stochastic modeling. *Journal of the atmospheric sciences* **53**, 1007-1017.

Kim, K.-Y., and Wu, Q. (1999). A comparison study of EOF techniques: Analysis of nonstationary data with periodic statistics. *Journal of Climate* **12**, 185-199.

Knapp, K. R., Kruk, M. C., Levinson, D. H., Diamond, H. J., and Neumann, C. J. (2010). The international best track archive for climate stewardship (IBTrACS). *Bulletin of the American Meteorological Society* **91**, 363.

Kopp, R. E. (2013). Does the mid-Atlantic United States sea level acceleration hot spot reflect ocean dynamic variability? *Geophysical Research Letters* **40**, 3981-3985.

Kopp, R. E., Horton, R. M., Little, C. M., Mitrovica, J. X., Oppenheimer, M., Rasmussen, D., Strauss, B. H., and Tebaldi, C. (2014). Probabilistic 21st and 22nd century sea-level projections at a global network of tide-gauge sites. *Earth's Future* **2**, 383-406.

LeSage, J. P. (2010). Econometrics toolbox. *Matlab software*.

Little, C. M., Horton, R. M., Kopp, R. E., Oppenheimer, M., and Yip, S. (2015). Uncertainty in Twenty-First-Century CMIP5 Sea Level Projections. *Journal of Climate* **28**, 838-852.

Liu, W., Huang, B., Thorne, P. W., Banzon, V. F., Zhang, H.-M., Freeman, E., Lawrimore, J., Peterson, T. C., Smith, T. M., and Woodruff, S. D. (2015). Extended reconstructed sea surface temperature version 4 (ERSST. v4): Part II. Parametric and structural uncertainty estimations. *Journal of Climate* **28**, 931-951.

Llovel, W., Cazenave, A., Rogel, P., Lombard, A., and Nguyen, M. (2009). Two-dimensional reconstruction of past sea level (1950-2003) from tide gauge data and an Ocean General Circulation Model. *Climate of the Past* **5**, 217-227.

Mahadevan, S., and Haldar, A. (2000). "Probability, reliability and statistical method in engineering design," John Wiley & Sons.

McPhaden, M. J., Zhang, X., Hendon, H. H., and Wheeler, M. C. (2006). Large scale dynamics and MJO forcing of ENSO variability. *Geophysical research letters* **33**.

Meyssignac, B., Becker, M., Llovel, W., and Cazenave, A. (2012). An assessment of two-dimensional past sea level reconstructions over 1950–2009 based on tide-gauge data and different input sea level grids. *Surveys in Geophysics* **33**, 945-972.

Oerlemans, J. (1989). A projection of future sea level. *Climatic change* **15**, 151-174.

Patwardhan, A., and Small, M. J. (1992). Bayesian methods for model uncertainty analysis with application to future sea level rise. *Risk analysis* **12**, 513-523.

Peltier, W. (2004). Global glacial isostasy and the surface of the ice-age Earth: the ICE-5G (VM2) model and GRACE. *Annu. Rev. Earth Planet. Sci.* **32**, 111-149.

Rayner, N., Parker, D. E., Horton, E., Folland, C., Alexander, L., Rowell, D., Kent, E., and Kaplan, A. (2003). Global analyses of sea surface temperature, sea ice, and night marine air temperature since the late nineteenth century. *Journal of Geophysical Research: Atmospheres* **108**.

Redmond, K. T., and Koch, R. W. (1991). Surface climate and streamflow variability in the western United States and their relationship to large-scale circulation indices. *Water Resources Research* **27**, 2381-2399.

Saha, S., Moorthi, S., Pan, H.-L., Wu, X., Wang, J., Nadiga, S., Tripp, P., Kistler, R., Woollen, J., and Behringer, D. (2010). The NCEP climate forecast system reanalysis. *Bulletin of the American Meteorological Society* **91**, 1015.

Saha, S., Moorthi, S., Wu, X., Wang, J., Nadiga, S., Tripp, P., Behringer, D., Hou, Y.-T., Chuang, H.-y., and Iredell, M. (2014). The NCEP climate forecast system version 2. *Journal of Climate* **27**, 2185-2208.

Simpson, M. J. R., Breili, K., and Kierulf, H. P. (2014). Estimates of twenty-first century sea-level changes for Norway. *Climate Dynamics* **42**, 1405-1424.

Slangen, A., Adloff, F., Jevrejeva, S., Leclercq, P., Marzeion, B., Wada, Y., and Winkelmann, R. (2016). A Review of Recent Updates of Sea-Level Projections at Global and Regional Scales. *Surveys in Geophysics*, 1-22.

Slangen, A., Carson, M., Katsman, C., Van de Wal, R., Köhl, A., Vermeersen, L., and Stammer, D. (2014). Projecting twenty-first century regional sea-level changes. *Climatic Change* **124**, 317-332.

Slangen, A., Katsman, C., Van de Wal, R., Vermeersen, L., and Riva, R. (2012). Towards regional projections of twenty-first century sea-level change based on IPCC SRES scenarios. *Climate dynamics* **38**, 1191-1209.

Stocker, T., Qin, D., Plattner, G., Tignor, M., Allen, S., Boschung, J., Nauels, A., Xia, Y., Bex, B., and Midgley, B. (2013). IPCC, 2013: climate change 2013: the physical science basis. Contribution of working group I to the fifth assessment report of the intergovernmental panel on climate change.

Van der Veen, C. (1988). Projecting future sea level. *Surveys in Geophysics* **9**, 389-418.

Wahr, J., Molenaar, M., and Bryan, F. (1998). Time variability of the Earth's gravity field: Hydrological and oceanic effects and their possible detection using GRACE. *Journal of Geophysical Research: Solid Earth* **103**, 30205-30229.

Whitaker, J. S., Compo, G. P., Wei, X., and Hamill, T. M. (2004). Reanalysis without radiosondes using ensemble data assimilation. *Monthly Weather Review* **132**, 1190-1200.

Woodruff, S. D., Worley, S. J., Lubker, S. J., Ji, Z., Eric Freeman, J., Berry, D. I., Brohan, P., Kent, E. C., Reynolds, R. W., and Smith, S. R. (2011). ICOADS Release 2.5: extensions and enhancements to the surface marine meteorological archive. *International journal of climatology* **31**, 951-967.

Yin, X., Gleason, B., Compo, G., Matsui, N., and Vose, R. (2008). The International Surface Pressure Databank (ISPD) land component version 2.2. *National Climatic Data Center: Asheville, NC. Available from ftp://ftp. ncdc. noaa. gov/pub/data/ispd/doc/ISPD2* **2**.

국문초록

CSEOF 를 이용한 한반도 주변 해역의 해수면 복원 및 전망

서울대학교 대학원
건설환경공학부
천세현

인공위성을 이용한 해수면 관측이 시작된 후 해수면에 대한 이해는 급속도로 발전해 왔다. 그러나 1992 년에 시작된 인공위성을 이용한 해수면 관측은 1800 년대에 시작된 조위소 관측 값에 비해 그 역사가 매우 짧다. 따라서 많은 연구들이 지구 전지역을 관측 범위로 하는 인공위성 자료의 관측 범위를 인공위성 관측 이전 시대로 확장하기 위해 인공위성 관측 자료와 조위소 자료를 동시에 이용한 해수면 복원에 대한 연구를 지속해 오고 있다. 그러나 이러한 연구의 대부분은 전지구적 관점에서 수행되어지고 있으며 이는 상대적으로 해수면의 변화의 폭이 작거나 조위 관측 지점이 숫자가 적은 지역에서의 해수면 복원의 정확성을 저하시키는 원인이 된다. 한반도 주변 해역의 경우 해수면 변화의 폭이 상대적으로 약하며 1960 년 이전의 조위 관측소의 숫자도 매우 부족한 실정이다. 따라서 본 연구에서는 한반도 주변해역에 대해 해수면 복원과 미래 해수면 변화 예측을 위한 새로운 방법을 제안하였다. 해수면 복원을 위해 CSEOF(Cyclo-Stationary Empirical Orthogonal Function) 분해를 통해 얻어진 LV(Loading Vector)를 지저함수(Basis function)로 사용하였으며 분해된 기저함수의 PCT(Principal Component Time series)를 1900 년 까지 연장하였다. 해수면 분해 자료의 PCT 를 확장하기 위해서는 복원된

해수면 온도 자료의 CSEOF 분해를 통해 얻어진 PCT 를 독립변수로 해수면의 PCT 를 종속변수로 한 시간 지연을 고려한 회귀분석이 이용되었다. 다양한 해수면 온도 자료를 활용해 총 13 개의 해수면 복원이 수행되었으며 북서태평양 지역의 COBESST2 를 이용한 복원이 조위소 관측을 통해 얻어진 해수면 값과 가장 높은 일치를 보였다. 본 복원에서는 한반도 주변의 조위소 관측 값이 사용되지 않았음에도 불구하고 조위소 관측 값을 사용한 이전 연구보다 높은 일치성을 보이고 있다. 본 연구에서는 인공위성 관측 자료를 기저함수로 사용하고 상응하는 PCT 를 미래로 연장해 해수면 값을 얻는 방식으로 미래 온실가스 배출 시나리오에 따른 해수면 예측 값을 산정하였다. 본 연구의 해수면 예측 방법은 기본적으로 해수면 복원 과정과 매우 유사하며 PCT 를 미래로 연장하기 위해 CMIP5 모델 중 하나인 HadGEM2-GE 모델의 해수면 온도 자료를 이용하여 PCT 를 미래로 연장 하였다. 해수면 예측은 RCP 시나리오 2.6, 4.5, 6.0, 그리고 8.5 에 대해서 2006-2100 년 기간에 대해서 수행하였다. 복원 및 예측된 해수면의 평균과 표준편차는 몬테 카를로(Monte Carlo) 시뮬레이션을 통해 각 월별 그리고 각 격자점에 대해서 계산되었다.

주요어: 해수면 상승, 인공위성 관측, 해수면 온도, 해수면 복원, 해수면 예측, CSEOF, 한반도

학번: 2013-30250